Phytomedicine 147 (2025) 157173

Contents lists available at ScienceDirect

Phytomedicine

journal homepage: www.elsevier.com/locate/phymed

Original Article

Oleandrin-mediated suppression of MELK induces apoptosis, autophagy, and ferroptosis in human non-small cell lung cancer cells

Ejlal A. Omer [a], Min Zhou [a], Wynand P. Roos [b], Luay J. Rashan [c], Heinz-Herbert Fiebig [d], Sabine M. Klauck [e], Letian Shan [f], Thomas Efferth [a,*]

[a] Department of Pharmaceutical Biology, Institute of Pharmaceutical and Biomedical Sciences Johannes Gutenberg University, Staudinger Weg 5, 55128 Mainz, Germany
[b] Department of Pathology and Laboratory Medicine, Warren Alpert Medical School & Legorreta Cancer Center, Brown University, Providence, RI 02912, United States
[c] Frankincense Biodiversity Unit, Research Center, Dhofar University, Salalah 211, Oman
[d] 4HF Biotec GmbH, Freiburg, Germany
[e] Division of Cancer Genome Research, German Cancer Research Center (DKFZ) Heidelberg, National Center for Tumor Diseases (NCT), NCT Heidelberg, a Partnership between DKFZ and University Hospital Heidelberg, 69120, Heidelberg, Germany
[f] The First Affiliated Hospital, Zhejiang Chinese Medical University, Hangzhou 310053, China

ARTICLE INFO

Keywords:
Natural products
Cardiac glycosides
Nerium oleander
NSCLC
Phytotherapy
Programmed cell death
In vivo

ABSTRACT

Background: Non-small-cell lung cancer NSCLC is the major diagnosed type of lung cancers in the USA and Europe. It is generally related to poor prognosis and low rates of survival. Oleandrin is a cardiac glycoside occurring naturally in *Nerium oleander* (Apocynaceae).
Purpose: To explore the potential therapeutic value of oleandrin against different cancer types with emphasis on NSCLC.
Methods: The effect of oleandrin in inhibiting the growth of different cancer cells was measured. In addition, oleandrin activity in inhibiting cell migration, suppression of MELK and inducing different modes of cell deaths were investigated using *in silico, in vitro*, and *in vivo* methods.
Results: Oleandrin showed activity at low nanomolar level against 17 different types of cancer cells including NSCLC. Our investigations in A549 cells indicated that oleandrin is a MELK inhibitor, as it disrupted the microtubule network and inhibited migration of A549 cells. Moreover, it induced apoptosis, autophagy, and ferroptosis. Furthermore, our *in vivo* data revealed that oleandrin had significantly decreased tumor growth in a A549 xenograft zebrafish model in a dose-dependent manner. *In silico* analyses revealed that oleandrin bound to the ligand binding pocket with higher binding affinity than the known inhibitor MELK-8a. The binding was further confirmed *in vitro* using microscale thermophoresis. An ADMET (absorption, distribution, metabolism, excretion, toxicity) analysis, together with our *in vivo* toxicity studies and the previous clinical studies suggest that oleandrin has an acceptable safety profile.
Conclusion: Oleandrin could potentially have therapeutic effects for NSCLC patients and possibly for other cancer types.

Introduction

Lung cancer is the second leading cause of death related to cancers in the USA. It is usually associated with poor prognosis and low survival rates. In the USA and Europe, >80 % of cases are histologically diagnosed as non-small cell lung cancer (de Jager et al., 2024; Siegel et al., 2023). The treatment approach for this type of cancer consists of surgery, radio-, immune-, and chemotherapy. Immunotherapy includes therapeutic antibodies such as PD-1 inhibitors (pembrolizumab, atezolizumab, cemiplimab, durvalumab, nivolumab), immune checkpoint inhibitors (tremelimumab, ipilimumab), and angiogenesis inhibitors (bevazimumab). Combination chemotherapy comprises classical

Abbreviations: ADMET, absorption-distribution-metabolism-excretion-toxicology; DMSO, dimethyl sulfoxide; MELK, maternal embryonic leucine zipper kinase; MOE, molecular operating environment; MST, microscale thermophoresis; NSCLC, non-small cell lung cancer; RT-qPCR, Real-time quantitative polymerase chain reaction; SCLC, small cell lung cancer.

* Corresponding author.
E-mail address: efferth@uni-mainz.de (T. Efferth).

https://doi.org/10.1016/j.phymed.2025.157173
Received 8 November 2024; Received in revised form 8 June 2025; Accepted 3 July 2025
Available online 15 August 2025

cytotoxic compounds such as cisplatin/ carboplatin, vinorelbine, pemetrexed, and paclitaxel (https://www.onkologie2024.de/#/inhalt/solidetumoren/b14lungenkarzinome/nichtkleinzelliges-lungenkarzinom-nsclc?q=lunge&tab=). For targeted chemotherapy small molecule drugs are used such as ALK tyrosine kinase inhibitors (ceritinib, crizotinib), and multi-kinase inhibitors (entrectinib) (Ettinger et al., 2022). Nevertheless, unfavorable side effects of cytotoxic and targeted drugs as well as therapeutic antibodies along with the risk of developing drug resistance drives the attention in oncological research towards the discovery of new molecules.

Since it has been characterized as a promising therapeutic target for multiple cancers, continuing research attempted to elucidate the role of maternal embryonic leucine zipper kinase (MELK) (Gray et al., 2005). MELK or murine protein Ser/Thr kinase 38 (MPK38) is a conserved kinase in the Snfl/AMPK family of serine/threonine kinases (Ganguly et al., 2015). This protein is overexpressed in different types of cancer including hepatic, ovarian, breast, cervical, colorectal, pancreatic, brain, bladder cancers and non-small cell lung cancer (NSCLC) (Chen et al., 2020; Kohler et al., 2017; Marie et al., 2008; Minata et al., 2014; Ni et al., 2024; Pickard et al., 2009; Wang et al., 2024; Xia et al., 2016).

In primary tumors and small cell lung cancer (SCLC) cell lines, MELK was identified as promising target for SCLC due to its frequent overexpression. The growth of all SCLC cell lines tested was inhibited by MELK knockdown or by treating the cells with the MELK inhibitor OTS167 (Inoue et al., 2016).

In NSCLC, the up-regulation of MELK, which is mediated by KLF5 and BBOX1-AS1, accelerated the progression of the disease. The malignant potential was reduced by treatment with the MELK inhibitor OTSSP167 (Shi et al., 2021). High levels of MELK can also aggravate lung adenocarcinoma because it controls EZH2 ubiquitination and H3K27me3 histone methylation of LATS2. Consequently, MELK silencing inhibited the tumor formation in nude mice (Yu et al., 2024).

In healthy cells, mitosis is tightly controlled. However, in cancer cells, it is frequently disturbed, leading to erroneous cell divisions and tumorigenesis. Antimitotic agents, including taxanes and *Vinca* alkaloids, are clinically well-established chemotherapeutics targeting microtubules. The eminent role of mitosis in cancer biology prompted the development of additional anti-mitotic drugs by addressing other mitosis-related targets such as mitotic kinesins, farnesyl transferase, heat-shock protein Hsp90, and the mitotic checkpoint (Dominguez-Brauer et al., 2015; Sudakin and Yen, 2007). Notably, in a cohort of stage 1 primary lung adenocarcinoma, the mitotic count was the only independent prognostic marker for survival (Duhig et al., 2015).

MELK is essential for mitotic progression in various cancers (Tang et al., 2020; Wang et al., 2018). Some studies linked MELK with metastasis and poor prognosis, because the knockdown of MELK impaired cell migration (Du et al., 2014; Xu et al., 2020). Moreover, radioresistance of cancer cells was associated with elevated expression of this protein (Choi and Ku, 2011; Kim et al., 2015; Speers et al., 2016). MELK is an essential oncogenic kinase in lung cancer, which controls metastasis (Speers et al., 2016). It contributed to the proliferation of stem-like cell-derived tumors (Liu et al., 2017; Nakano et al., 2005). Besides, it inhibited apoptosis by interacting with pro-apoptotic Bcl-2 family members (Lin et al., 2007). Notably, the growth of cancer cells was effectively inhibited by the prototype MELK inhibitors NVS-MELK8a and OTS167 (Alachkar et al., 2014).

Oleandrin is a cardiac glycoside naturally present in all parts of the oleander tree (*Nerium oleander* L., Apocynaceae). Oleandrin has been used in traditional medicine for the treatment of a wide range of illnesses, such as scabies, strokes, control of fertility, sores, dermatitis, epilepsy, herpes, and leprosy (Dunn et al., 2011; Lans, 2007; Murshed et al., 2024; Zhai et al., 2022). Furthermore, oleandrin has demonstrated different *in vitro* activities, including cardioprotective (Gayathri et al., 2011), antimicrobial (Bhuvaneshwari et al., 2007), and anticonvulsant effects (Singhal and Gupta, 2011) as well as larvicidal and mosquitocidal effects against Plasmodia (El-Akhal et al., 2015; Fakoorziba et al., 2015), anti-poliovirus (Sanna et al., 2021), SARS-CoV-2 inhibitory activity (Plante et al., 2021), and most importantly, anticancer activity. Recently, our research group revealed that a standardized leaf extract from *Nerium oleander*L. (termed "Breastin") was cytotoxic towards 14 hematopoietic tumor cell lines (multiple myeloma, leukemia) and cell lines derived from solid tumors (Rashan et al., 2023).

Here, we are continuing our studies on *N. oleander* as anticancer agent. Therefore, we aimed to investigate the anticancer activity of oleandrin as a principal toxic and pharmacologically active constituent in this plant (Langford and Boor, 1996) by treatment of different cancer cell lines. Specifically, we explored the MELK inhibitory effect of oleandrin in lung cancer cells.

Materials and methods

Chemicals

Oleandrin 98 % (CAS:465–16–7) was purchased from Cymit Quimica SL. (Barcelona, Spain).

Cell lines

The 40 cell lines of the Oncotest panel used in this investigation have been described (Fiebig et al., 1992; Roth et al., 1999).

The lung cancer cells A549 ATM$^{+/+}$ and A549 ATM$^{-/-}$ were kindly provided by Prof. Susan P. Lees-Miller (Charbonneau Cancer Institute, University of Calgary, Canada). Both lung cancer cells H460 MSH6$^{+/+}$ and H460 MSH6$^{-/-}$ were provided by Prof. Anatoly Zhitkovich (Brown University, Department of Pathology and Laboratory Medicine, Providence, Rhode Island). The drug-sensitive CCRF-CEM T-ALL and their counterpart multidrug-resistant P-glycoprotein-overexpressing CEM/ADR5000 leukemia cells were obtained from Dr. Axel Sauerbrey (Children's Hospital, University of Jena, Germany). The glioblastoma cells U87.MG and its drug-resistant U87.MGΔEGFR subline were supplied by Webster K. Cavenee (Ludwig Institute for Cancer Research, University of California at San Diego, La Jolla, *CA*, USA). The HCT116 (p53$^{+/+}$) colorectal cancer cells and their knockout clones HCT116 (p53$^{-/-}$) were a gift from Dr. B. Vogelstein and H. Hermeking (Howard Hughes Medical Institute, Baltimore, MD). Both MDA-MB-231 BCRP and MDA-MB-231 PARP3$^{-/-}$ breast cancer cells were generously provided by Prof. Françoise Dantzer (Universite de Strasbourg, Institute de Recherche de l'Ecole de Biotechnologie de Strasbourg, France). The multiple myeloma cell lines AMO1 and OPM2 were obtained from Dr. Manik Chatterjee and Dr. Ellen Leich (University of Würzburg, Germany). Both B16-F1 cells and B16-F10 cells were provided by Prof. Ugur Sahin (TRON-Translational Oncology at the University Medical Center of Johannes Gutenberg University GmbH, Mainz, Germany), SK-MEL-505 melanoma cells and wild-type U2OS osteosarcoma cells were provided by Dr. Wynand P. Roos (Institute of Toxicology, Medical University Center, Mainz, Germany). U2OS cells stably transfected with GFP-α-tubulin fusion cDNA were obtained by Dr. Joachim Hehl (Light Microscopy Centre, ETH, Zurich, Switzerland). The melanoma cells MaMel-80a cells and Mel-2A cells were supplied by Prof. David Schrama (Department of Dermatology, Julius-Maximilians University, Würzburg, Germany). The kidney embryonic cells HEK293/ABCB5 were obtained from Prof. Yoshikazu Sugimoto (Division of Chemotherapy, Faculty of Pharmacy, Keio University, Tokyo, Japan). AML12 normal hepatocytes were obtained from the American Type Cell Culture Collection ATCC (USA). The MRC-5 normal lung fibroblasts were supplied by Dr. rer. nat. Sebastian Zahnreich (University Medical Center Mainz, Germany).

The SK-MEL-28, MaMel-80a and SK-MEL-505 melanoma cell lines, H460 MSH6$^{+/+}$ and H460 MSH6$^{-/-}$ lung cancer cell lines, as well as CCRF-CEM and CEM/ADR5000 T-acute lymphoblastic leukemia cells were cultured in RPMI-1640 (Life Technologies, Darmstadt, Germany) supplemented with 10 % FBS (Life Technologies) and 1 % penicillin

Table 1
The sequences of qRT-PCR primers (5′ to 3′).

Genes	Forward primer	Reverse primer
CXCL5	AGCTGCGTTGCGTTTGTTTAC	TGGCGAACACTTGCAGATTAC
TFPI2	TCCTGCCCCTAGACTACGG	CTCCCAGGTGTAGAAATTGTTGG
EIF1	GAAACGGCAGGAAGACCCTTA	CGGATGCTCAATTACAGTACCAT
EIF5	TTAATCGGCCTCCAACGTATCC	CTTGCAGCTTATTCGCCTCAT
CCT3	AAGTCCATGATCGAAATTAGCCG	TGCTCAGCTACAGACAGCATT
RPL41	GGAAACCTCTGCGCCATGA	CCCACAACTTGTACCAGCATCC
GAPDH	CCCCAGCAAGAGCACAAGAGGAAGAG	TGATGGTACATGACAAGGTGCGG
MELK	CTCCGCCCCTCAGAGTGATT	AGCTCTCCTCCAGGGCAGTA
GPX4	CCCGCTGTGGAAGTGGATGA	TGTGGAGAGACGGTGTCCAA
ACSL4	CGAGCTTTCCGAGTGCCAG	CAGTACAGCCAAGGCAGTTCAAT
TRFC	ACCATTGTCATATACCCGGTTCA	CAATAGCCCAAGTAGCCAATCAT
BECN11	TGGGGAGGTTAGGATTTGGGA	GAGCCGTAGGGTGGAAAGC
ATG5	AGCCGGAAGGAGGAGCCATA	TCGTCCAAACCACACATCTCG
SQSTM1	GATTCGCCGCTTCAGCTTCT	AAAGGCAACCAAGTCCCCGT

(1000 U/ml)/streptomycin (100 µg/ml) (Life Technologies). All other cell lines were cultured in DMEM (Life Technologies) enhanced with 10 % FBS (Life Technologies) and 1 % penicillin (1000 U/ml)/streptomycin (100 µg/ml) (Life Technologies). The cells were incubated in 5 % CO_2 at 37 °C.

Samples of fresh blood were collected from three healthy donors at the Department of Hematology, Oncology, and Pneumology (University Medical Center of the Johannes Gutenberg University, Mainz, Germany). The samples were kept in plastic Monovette EDTA tubes. Human peripheral blood mononuclear cells (PBMCs) were isolated using Histopaque® (Sigma-Aldrich, Taufkirchen, Germany). Aliquots of fresh blood (3 ml) were added carefully at the top of Histopaque® and centrifuged at 400 × *g* for 30 min. Afterward, the PBMC-containing layer was separated, washed three times with PBS, and centrifuged at 250 × *g* for 10 min. The PBMCs were suspended in Panserin 413 growth media (PAN-Biotech, Aidenbach, Germany) with 2 % phytohemagglutinin M (PHA-M, Life Technologies).

Cell viability assays

Propidium iodide cell viability assay: A modified propidium iodide assay was used to assess the compound's activity in Oncotest's panel of 40 tumor cell lines (Dengler et al., 1995; Rashan et al., 2023).

Resazurin reduction assay: The cell viability of cells was studied using the cell-permeable redox indicator resazurin. Aliquots of 100 µl of growth medium were used to suspend 1×10^4 or 5×10^3 cells per well for suspended or adherent type of cells, respectively, in a flat bottom 96-well plate. The cells were then treated with 100 µl medium containing different concentrations of oleandrin. Serial dilutions of oleandrin in DMSO were prepared. The final concentration was ranging from 3 nM to 500 nM in a final volume of 200 µl/ well. Cells treated with 0.5 % of DMSO were considered as negative control. The plates were incubated for 72 h at 37 °C and 5 % CO_2. Resazurin 0.01 % *w/v* (Sigma–Aldrich, Darmstadt, Germany) was added and incubated for 4 h. The fluorescence produced by the reduction of resazurin by living cells was measured using an Infinite™ M2000 Pro plate reader (Tecan, Crailsheim, Germany).

The resazurin assay was also used to investigate the influence of the ferroptosis inhibitor ferrostatin-1 on A549 cells treated with oleandrin, as previously described (Mbaveng et al., 2019). Aliquots of 5×10^3 cells/well were cultured with ferrostatin-1 (50 µM) for 1 h before exposure to treatment. Subsequently, cells incubated with different concentrations of oleandrin were incubated for 48 h in a 5 % CO_2 environment at 37 °C, and resazurin solution (20 µl 0.01 % *w/v*) was added to each well and incubated in the dark for a further 4 h. The Infinite™ M2000 Pro plate reader was used for fluorescence measurement.

The IC_{50} value of various cell lines based on a calibration curve was determined by exponential linear regression analysis using Microsoft Excel. The results were given as mean ± SD of at least three different independent trials with each six parallel measurements for each calculated IC_{50}.

Transcriptomics

A549 cells were subjected to either DMSO or 6.98 nM oleandrin (= IC_{50}) and incubated for 24 h. RNA was extracted using InviTrap® Spin Universal RNA Mini Kit (stratec Molecular GmbH, Berlin, Germany). The process of quality control of total RNA, probe labelling, scanning, hybridization, and data analysis of the samples was performed at the Genomics and Proteomics Core Facility of the German Cancer Research Center (DKFZ, Heidelberg, Germany). Microarray hybridizations were performed using Affymetrix GeneChips® with human Clariom™ S assays (Affymetrix, Santa Clara, *CA*, USA) (Boulos et al., 2023b).

The results were analysed using Chipster software (version 3.16.3) to compare the differentially expressed genes in the treated and untreated groups. The resulting filtered genes were analysed using the core analysis tool of the Ingenuity Pathway Analysis (IPA) software (Qiagen, Redwood City, *CA*, USA) to determine the effect of oleandrin.

Real-time quantitative polymerase chain reaction (RT-qPCR)

One microgram of the extracted RNA was converted to cDNA following the manufacturer guidelines of the LunaScript® RT SuperMix Kit (NEB #E3010) (New England Bio Labs, Darmstadt, Germany). The PCR primers were designed using PrimerBank (harvard.edu) (Wang et al., 2012), proven with the Oligo Analysis Tool from Eurofins Genomics Germany GmbH (Ebersberg, Germany), and purchased from this supplier. The sequences of the primers are shown in Table 1.

The primers were mixed with 5 × Hot Start Taq EvaGreen® qPCR Mix (Axon-Labortechnik, Kaiserslautern, Germany) and the cDNA following the manufacturer instructions and then subjected to CFX384™ Real-Time PCR (Bio-Rad Laboratories GmbH, Feldkirchen, Germany), using *GAPDH* as control gene. Each sample in duplicates was measured at least three times.

Expression data of the target gene were displayed as fold change adjusted to the *GAPDH* gene for the DMSO only treated control sample. Regarding the test sample, the gene expression fold change in comparison to the untreated control is revealed by the analysis of 2ˆ-ddct after normalization to the *GAPDH* gene.

To verify the results obtained from microarray hybridization, we exemplarily selected three upregulated genes and three downregulated ones (*CXCL5, TFPI2, EIF1, RPL41, CCT3,* and *EIF5*). Besides those genes, we also detected MELK, three of autophagy-related genes (*BECN1, ATG5*, and *SQSTM1*/p62) and three of ferroptosis-related genes (*GPX4, ACSL4,* and *TRFC*).

Single-cell electrophoresis (comet) assay

We performed single-cell gel electrophoresis comet assays using a described protocol (Olive and Banáth, 2006) and U2OS cells. The cells were treated with oleandrin concentrations equivalent to 0.5 IC_{50}, IC_{50}, 2 × IC_{50}, and 4 × IC_{50} for 48 h. Untreated cells served as a negative control, whereas cells treated with 150 μM of tert-Butyl hydroperoxide (t-BuOOH) for 1 h served as a positive control. Cells were embedded in 0.5 % low melting point agarose in PBS and spread onto glass slides coated with 1.2 % agarose. Cells were lysed in lysing solution (for neutral comet: 2.5 M NaCl, 100 mM EDTA, 10 mM Tris, 1 % Na-laurylsarcosinate, 1 % Triton X-100, pH 7.5. For alkaline comet: 2.5 M NaCl, 100 mM EDTA, 10 mM Tris, 1 % Tryton-X100, pH 10). For neutral comet, slides were electrophoresed for 25 min in electrophoresis buffer (90 mM Tris pH 7.5, 90 mM boric acid, 2 mM EDTA) at 7.4 V/cm. For alkaline comet, DNA was allowed to unwind for 20 min in electrophoresis buffer (0.3 N NaOH, 6 mM EDTA, pH > 13) followed by 15 min electrophoresis at 25 Volts and 300 mA. Slides were fixed in 100 % methanol and then air-dried. DNA was stained using propidium iodide (50 μg/ml) and 50 cells per slide were evaluated randomly using a fluorescence microscope and the Comet IV software (Perceptive Imaging, Liverpool, UK). Data are expressed as tail intensity, which denotes the percentage of DNA in the tail multiplied by the length between the center of the head and tail.

Western blotting

A549 cells were treated with oleandrin equivalent to 0.5 IC_{50}, IC_{50}, 2 × IC_{50}, and 4 × IC_{50} concentrations. After 48 h incubation, total protein was extracted with M-PER Mammalian Protein Extraction Reagent (Thermo Fisher Scientific, Darmstadt, Germany) as previously described (Zhou et al., 2023). Protein samples (30 μg) were separated using 10 % SDS-PAGE gel electrophoresis and then transferred to a PVDF membrane. The membrane was blocked at room temperature for 1 h using 5 % BSA, then incubated overnight with the primary antibody at 4 °C. The following antibodies were used: MELK rabbit antibody (1:1000, Cell Signaling Technology, Leiden, Netherlands), caspase-3 rabbit antibody (1:1000, Cell Signaling Technology) and GAPDH rabbit antibody (1:1000, Cell Signaling Technology). The membrane was incubated with secondary anti-rabbit IgG HRP-linked antibody (1:1000, Cell Signaling Technology) for 1 h at room temperature. After treating the membrane with Luminata™ Classico Western HRP substrate (Merk Millipore Darmstadt, Germany), an Alpha Innotech FluorChem Q System (Biozym, Oldendorf, Germany) was used to visualize the bands. ImageJ software V5 (National Institute of Health, Bethesda, MD, USA) was applied to quantify the expression of the protein compared to untreated control.

Imaging the microtubule cytoskeleton by fluorescence confocal microscopy

Aliquots of 3 × 10^4 U2OS-GFP-α-tubulin cells were seeded on μ-Slide 8 Well (ibidi GmbH, Gräfelfing, Germany), and incubated overnight at 37 °C, 5 % CO_2. Afterwards, the cells were treated with concentrations equivalent to 0.5 IC_{50}, IC_{50}, 2 × IC_{50}, and 4 × IC_{50} of oleandrin. Untreated cells served as negative control. Vincristine (0.25 μM, polymerization inhibitor) and paclitaxel (0.5 μM, depolymerization inhibitor) were used as positive controls. After 24 h incubation, the cells were washed with PBS, fixed with 4 % paraformaldehyde for 15 min. Following that, the cells were washed three times with PBS. The nucleus was stained with 4′,6-diamidino-2-phenylindole (DAPI, 1 μg/ml; Sigma–Aldrich, Darmstadt, Germany). The cells were washed three times with PBS, and ibidi mounting medium (ibidi, Gräfelfing, Germany) was applied to all slides. The AF7000 widefield fluorescence microscope (Leica Microsystems, Wetzlar, Germany) was used for imaging. GFP and DAPI were both excited by the blue laser (λ/nm = 470). The emission wavelengths were λ/nm = 525, λ/nm = 447 for GFP and DAPI, respectively. The images were analyzed using ImageJ software.

Detection of cell migration by in vitro scratch assay

An *in vitro* wound healing assay was used to test cell migration as previously described (Grada et al., 2017). Briefly, 0.2 × 10^6 A549 cells/well were seeded in a 12-well plate. After overnight incubation, the cells attached as monolayer. A sterile 10 μl pipette tip was used to create cell-free zone across the cell monolayer in each well. The cells were treated with oleandrin equal to 0.5 IC_{50}, IC_{50}, 2 × IC_{50}, and 4 × IC_{50} concentrations. Imaging was performed with a JuLIT™ Br Live Cell Movie Analyzer (NanoEnTek Inc., Seoul, Korea), with a 4× magnification object at T0, 24 h and 48 h. Image J software was used to measure the wound area. The experiment was repeated three times independently. The percentage of wound closure was calculated as follows:

$$\text{Wound Closure \%} = \frac{A_{t=0h} - A_{t=\Delta h}}{A_{t=0h}} * 100\%$$

$A_{t=0\ h}$ is the area of the wound measured immediately after scratching.
$A_{t=\Delta h}$ is the area of the wound measured in *h* (hours) after the scratch is performed.

Detection of apoptosis

The Violet Ratiometric Membrane Asymmetry Probe/Dead Cell Apoptosis Kit (Thermo Fisher Scientific, Darmstadt, Germany) was used to detect apoptosis in A549 cells. The kit was used following the manufacturer instructions. Briefly, 0.3 × 10^6 cells were seeded in a 6-well plate and then treated the next day with different concentrations of oleandrin (0.5 IC_{50}, IC_{50}, 2 × IC_{50}, and 4 × IC_{50}). After an incubation period of 48 h in 5 % CO_2, 37 °C, the cells were harvested and washed twice with 1 ml of cold Hank's balanced salt solution (HBSS), and finally resuspended in 1 ml of HBSS. Afterward, 1 μl F2N12S solution was added to each sample at a final concentration of 200 nM. Another 1 μl SYTOX® AADvanced™ dead cell stain solution was added at a final concentration of 1 μM. Untreated cells were used as negative control whereas camptothecin-treated cells (10 μM) were used as positive control. The samples were analysed after 5 min incubation using Novocyte Quanteon (Agilent). In linear scale, the cells were gated SSC-A/ FSC-A. The single cell gating was achieved by SSC—H/ SSC-A. F2N12S was excited by the violet laser (405 nm) and fluorescence emission was detected using the orange fluorescence channel (586/20 bandpass filter) and the green fluorescence channel (525/45 bandpass filter). Both parameters were recorded on linear scale. SYTOX® AADvanced™ was used for staining dead cells and was excited with a yellow-green laser (561 nm) and emitted light was collected using a 695/40 bandpass filter. Using FlowJo software (v10.10), the ratio of the orange fluorescence channel to the green fluorescence channel was set as a derived parameter. The amount of living, apoptotic and dead cells was quantified. Three independent replications of the experiment were performed.

Detection of autophagy

Autophagy was analyzed using the Autophagy Detection Kit (ab139484, Abcam, Cambridge, UK) following the manufacturer instructions. The method was described previously (Boulos et al., 2023a). Briefly, 0.3 × 10^6 of A549 cells were seeded in each well of a 6-well plate, incubated overnight, then treated with oleandrin concentrations equivalent to 0.5 × IC_{50}, IC_{50}, 2 × IC_{50} and 4 × IC_{50}. The positive control rapamycin was added 18 h before analysis. After 48 h incubation time, the cells were collected and washed with PBS, resuspended in 250 μl of PBS with 5 % FBS. Green stain (250 μl; 1: 1000 in PBS with 5 %FBS) was added. The samples were incubated at 37 °C for 30 min. Later, the cells were collected by centrifugation, washed with assay buffer and resuspended in 500 μl of the assay buffer. The samples were analyzed with an Accouri C6 flow cytometer (Becton-Dickinson, Heidelberg, Germany)

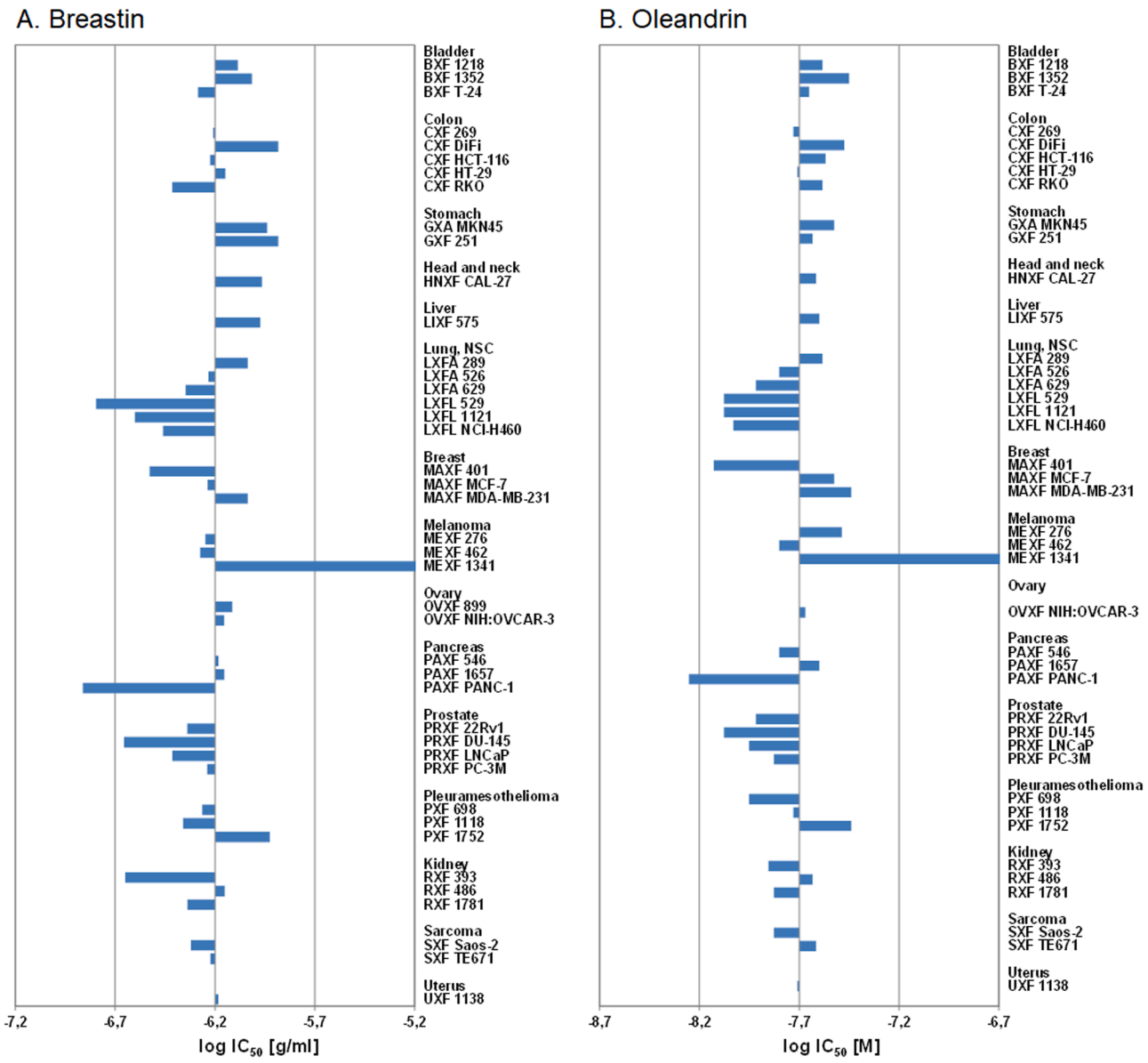

Fig. 1. Comparison of IC_{50} values for 40 cell lines of different tumor origin from the Oncotest panel towards (A) Breastin and (B) oleandrin. The IC_{50} values for each cell line have been calculated from dose response curves. The individual IC_{50} values for each cell line have been used to calculate the mean IC_{50} value. The IC_{50} values of cell lines sensitive to Breastin or oleandrin were plotted as bars to the left side, those of resistant cell lines to the right side. The x-axis shows log IC_{50} whereas the y-axis shows the cell lines tested. The pattern of IC_{50} similarity among the 40 cell lines was calculated by using the Spearman correlation test ($r = 0.84$).

using a 530/30 nm band pass filter to detect green fluorescence. A total of 10^4 events were recorded per histogram. The gating strategy applied was FSC-A/SSC-A gate for living cells and FSC-A/ FSC—H for singlets. The analysis and graph generation were performed using FlowJo software. The experiment was repeated three times independently.

Molecular docking

Molecular Operating Environment (MOE, 2022.02, Chemical Computing Group Montreal, Canada) was used for the docking study. The crystal structure of MELK co-crystalized with NVS-MELK8a (PDB: 5IH9) was used for docking of both oleandrin and its metabolite oleandrigenin. The MELK inhibitor NVS-MELK-8a served as control. The protein was prepared for docking, hydrogens were added, and the protonation states were assigned. These steps were performed by default with the software. The energy of the protein and of each ligand was minimized. The binding pocket was identified using site finder. All molecules were docked to the NVS-MELK8a binding site. Induced fit model was selected. We executed 100 poses for each process and 50 refinements for each ligand. The scoring energy values were predicted by utilizing London dG scoring function. The results were expressed as S scores (the lower the score the stronger the binding affinity of the compound to the receptor). 2D interactions of amino acids with ligands were shown by MOE, whereas the 3D figures were generated using BIOVIA Discovery Studio visualizer (https://discover.3ds.com/discovery-studio-visualizer-download).

Microscale thermophoresis (MST)

Recombinant MELK protein (Cat: M50–18 G) was purchased from Sino Biological (Düsseldorf, Germany). The protein was labelled using the Monolith™ NT.115 Protein Labeling Kit BLUE-NHS (NanoTemper Technologies GmbH, Munich, Germany). The concentration of the labelled protein was determined using Nanodrop (Thermo Fisher

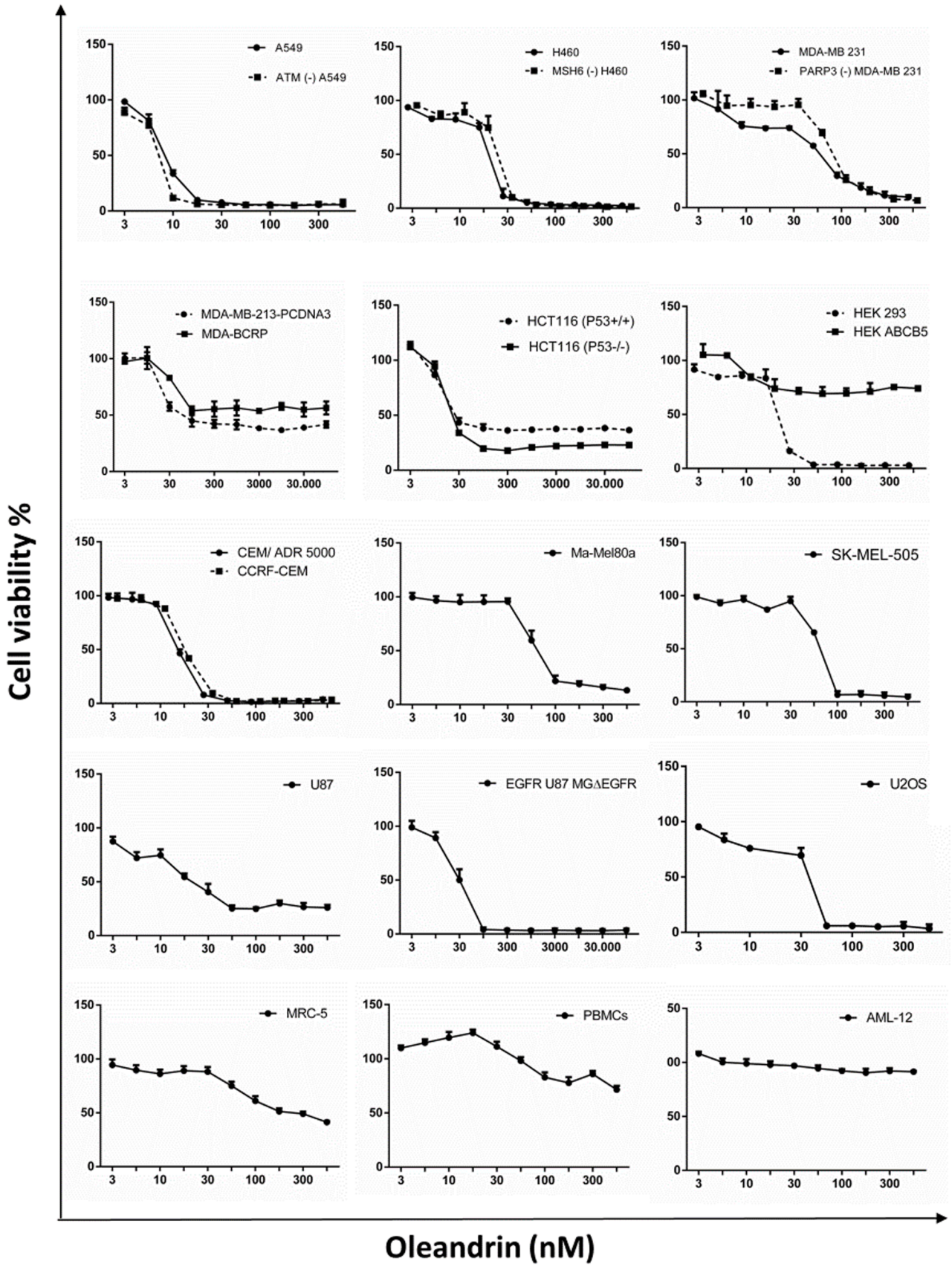

Fig. 2. Growth-inhibitory effect of oleandrin towards 17 different human cancer cell lines in addition to two human kidney embryonic cell lines (HEK293, HEK293-ABCB5), and three normal cell types (human MRC-5 cell line, human PBMCs, and murine AML-12 cell line) as measured by the resazurin assay. The x-axis shows the concentration of oleandrin in nM, whereas the y-axis shows cell viability %. The results are shown as mean values ± SD of three independent experiments containing six replicates each.

Scientific). The binding assay was executed as described previously (Omer et al., 2023). Sixteen serial dilutions of oleandrin were prepared in assay buffer (50 mM Tris buffer, pH 7.4 containing 150 mM NaCl, 10 mM $MgCl_2$, and 0.05 % Tween-20). The starting concentration was 300 μM. The labelled protein was added to each dilution (1:1) and incubated for at least 5 min at room temperature. Using capillaries, the 16 samples were loaded to NanoTemper Monolith™ NT (NanoTemper Technologies GmbH, Munich, Germany). LED (Light Emitting Diodes) power was set to 80 % whereas the laser power was adjusted to 20, 40 and 60. The data were analyzed using MO. Affinity Analysis software generated the fit curve. The dissociation constant (K_d) was calculated as mean of three independent experiments.

Xenograft animal assay

China Zebrafish Resource Center (CZRC) in Wuhan, China, provided the wild-type AB strain of zebrafish. The *in vivo* experiments were approved by the Association for Assessment and Accreditation of Laboratory Animal Care International (SYXK, 2012–0171). The larval zebrafish, which were obtained through natural pair-mating two days after fertilization, were raised in light-controlled fish farming water with the following parameters: pH 6.9–7.2, conductivity 480–510 μS/cm, salinity 200 mg/l instant sea salt, photoperiod 14:10 h day/night, and temperature 28 °C. The fish were fed brine shrimp twice a day in addition to fry flakes once a day.

A549 cells were labelled with the fluorescent cellTracker™ CM-Dil dye (Thermo Fisher Scientific, Leiden, Netherlands) according to the manufacturer's protocol. To create a xenograft model in zebrafish 200 cells/fish were injected into the larvae yolk sac 48 h after fertilization (Zhang et al., 2021). Tumor growth in the model was assessed 24 h later, the fluorescence intensity (FI) of the A549 transplanted tumor was measured by a motorized fluorescent microscope with continuous zoom (AZ100, Nikon,Tokyo, Japan). Different concentrations of oleandrin were used for treatment of the created model for 24 h. The following formula was applied to calculate the inhibitory rate:

inhibitory rate %= [1 - (FI of treated group/FI of untreated group)] × 100 %.

$n = 10$ zebrafishes, FI= fluorescence intensity

Results

Inhibition of cell viability by oleandrin

We first compared the responsiveness of 40 tumor cell lines from the Oncotest panel towards a cold-water extract of *Nerium oleander* termed Breastin with a main ingredient, oleandrin, using a propidium iodide-based cell viability assay. The IC_{50} values that have been calculated from dose response curves of all cell lines were used to determine the mean IC_{50} values. As shown in Fig. 1, the *in vitro* activity of oleandrin (IC_{50} = 0.026 μM, equivalent to 0.015 μg/ml) was 64-fold higher compared to Breastin (IC_{50} = 0.961 μg/ml). The IC_{50} values of the cell lines smaller than the mean value were plotted as bar to the left side. These were the sensitive cell lines. The IC_{50} values of the resistant cell lines were plotted to the right side. The IC_{50} profiles across the cell lines treated with Breastin (Fig. 1A) and oleandrin (Fig. 1B) were visually similar. To quantify the extend of similarity, we subjected the IC_{50} values to the Spearman correlation test and obtained a correlation coefficient of $r = 0.84$, indicating a high degree of similarity. Some of the cell lines were particularly sensitive to both Breastin and oleandrin, *e.g.*, the lung cancer cell lines LXFL 629, LXFL 529, LXFL 1121, and LXFL NCI-H460, the pancreas cancer cell line PAXF PANC-1, the prostate cancer cell line PRXF DU-145, as well as the kidney cancer cell line RXF 393.

Table 2
IC_{50} values of tumor cell lines and normal cells upon treatment with oleandrin.

Cell type	Cell line	IC_{50} (nM)
Lung cancer	A549 $ATM^{+/+}$	6.98 ± 1.28
Lung cancer	A549 $ATM^{-/-}$	6.65 ± 0.45
Lung cancer	H460 $MSH6^{+/+}$	19.72 ± 0.61
Lung cancer	H460 $MSH6^{-/-}$	19.42 ± 1.53
T-acute lymphoblastic leukemia	CCRF-CEM	13.96 ± 0.12
T-acute lymphoblastic leukemia	CEM/ADR5000	14.58 ± 0.42
Glioma	U87.MG	19.72 ± 0.25
Glioma	U87.MG-ΔEGFR	30.42 ± 0.00
Colorectal cancer	HCT116 $p53^{+/+}$	25.15 ± 0.00
Colorectal cancer	HCT116 $p53^{-/-}$	22.15 ± 2.25
Breast cancer	MDA-MB-231	60.20 ± 1.73
Breast cancer	MDA-MB-231 pcDNA3	55.43 ± 0.01
Breast cancer	MDA-MB-231 BCRP	>500
Breast cancer	MDA-MB-231 $PARP3^{-/-}$	68.14 ± 3.54
Osteosarcoma	U2OS	37.19 ± 3.40
Multiple myeloma	AMO1	>500
Multiple myeloma	OPM2	>500
Melanoma (murine)	B16-F1	>500
Melanoma (murine)	B16-F10	>500
Melanoma	SK-MEL-28	>500
Melanoma	MaMel-80a	55.58 ± 8.21
Melanoma	Mel-2A	>500
Melanoma	SKMEL-505	59.62 ± 0.79
Kidney embryonic cells	HEK293	21.11 ± 0.57
Kidney embryonic cells	HEK293-ABCB5	>500
Normal peripheral blood mononuclear cells	PBMC	>500
Normal hepatocytes (murine)	AML-12	>500
Normal lung fibroblasts	MRC-5	248.7 ± 0.08

As a next step, the cytotoxicity of oleandrin was tested using a second method, the resazurin reduction assay, against a broad panel of different human cancer cell lines derived from lung cancer (A549 $ATM^{+/+}$, A549, $ATM^{-/-}$, H460 $MSH^{+/+}$, and H460 $MSH6^{-/-}$), multiple myeloma (AMO1 and OPM2), T-acute lymphoblastic leukemia (CCRF-CEM and CEM/ADR5000), melanoma (SK-MEL-28, MaMel-80a, Mel-2A, SK-MEL-505), osteosarcoma (U2OS), breast cancer (MDA-MB 231 and MDA-MB-213-pcDNA3, MDA-MB-231-BCRP, MDA-MB-231 $PARP3^{-/-}$), glioma (U87. MG and U87. MGΔEGFR), and colorectal cancer (HCT116 $p53^{+/+}$ and HCT116 $p53^{-/-}$). We also applied the compound to two cell lines of murine melanoma (B16-F1 and B16-F10), as well as normal cells including human embryonic kidney cells (HEK293) and HEK-ABCB5, human peripheral blood mononuclear cells (PBMCs), the human lung fibroblast cell line MRC-5, and the murine hepatocyte cell line AML-12.

Oleandrin showed activity at low nanomolar levels against almost all cancer cell lines tested. The lowest IC_{50} was found in A549 $ATM^{-/-}$ lung cancer cells (IC_{50}: 6.65 ± 0.45 nM), the highest in MDA-MB-231 $PARP3^{-/-}$ cells (IC_{50}: 68.14± 3.54 nM) (Fig. 2, Table 2).

Oleandrin did not affect the viability of some other cell lines up to a concentration of 500 nM, *i.e.*, AMO1 and OPM2 multiple myeloma cells, human and murine SK-MEL-28, Mel-2A, B16-F1, and B16-F10 melanoma cells, as well as HEK-ABCB5 and MDA-MB-231-BCRP cells. Importantly, oleandrin was also inactive on normal cells, besides the

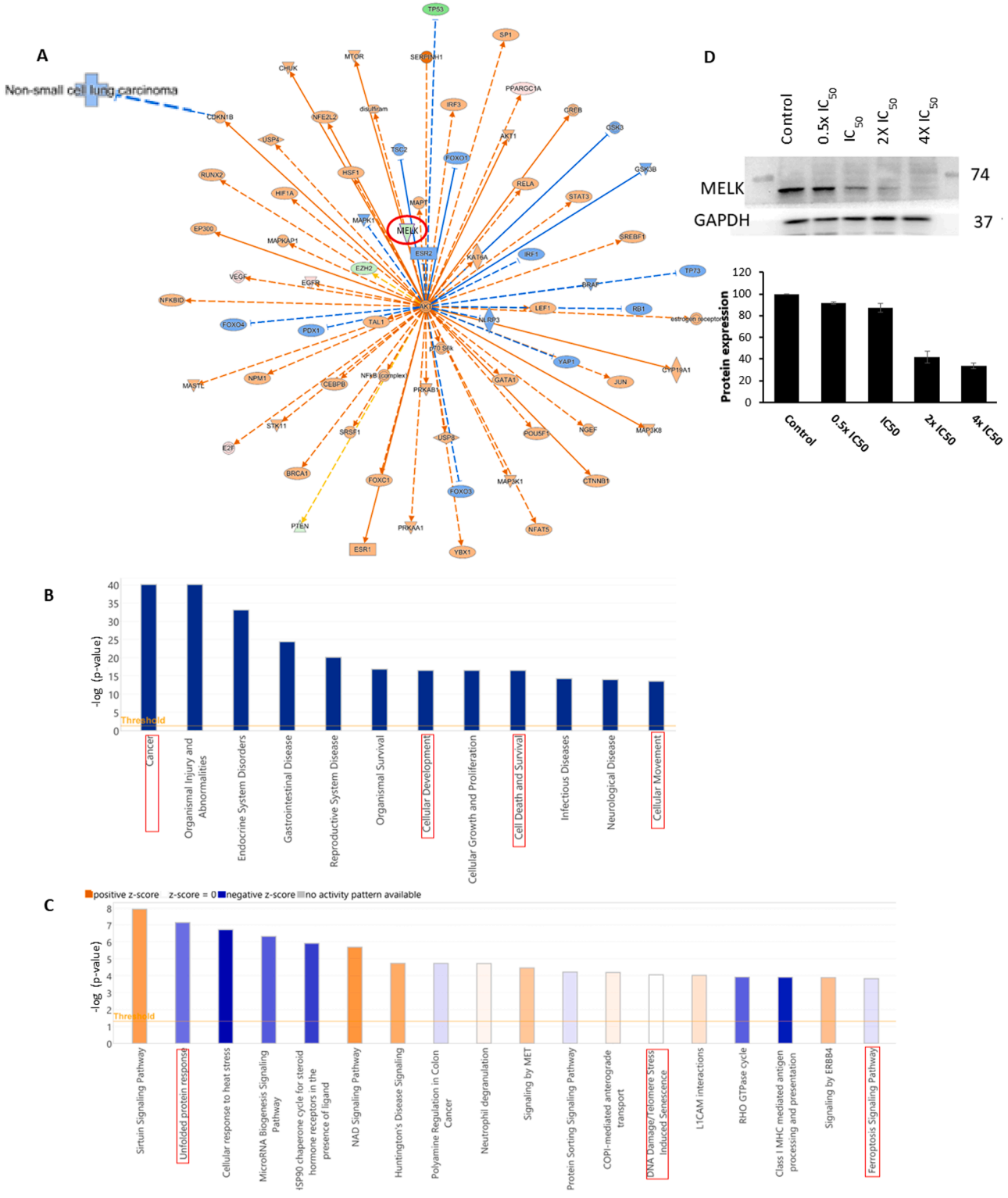

Fig. 3. Ingenuity Pathway Analysis (IPA) of gene expression profiling of A549 cells. The cells were treated with the IC_{50} concentration of oleandrin for 24 h. (A) Prediction of a functional network for NSCLC. (B) Top cellular functions and diseases affected by oleandrin. (C) Canonical pathways. A cut-off threshold of 1.3 was considered for –log (*P* value). (D) Western blotting analysis and quantification of MELK protein expression. The bar diagrams were obtained from the calculation of the mean value ± SD of three independent experiments performed at different time points.

HEK293 cell line (Table 2).

MELK downregulation in oleandrin-treated A549 cells as determined by microarray hybridization

We used mRNA microarray hybridization to assess differential gene expression in the lung cancer cell line A549 $ATM^{+/+}$ (short A549) with

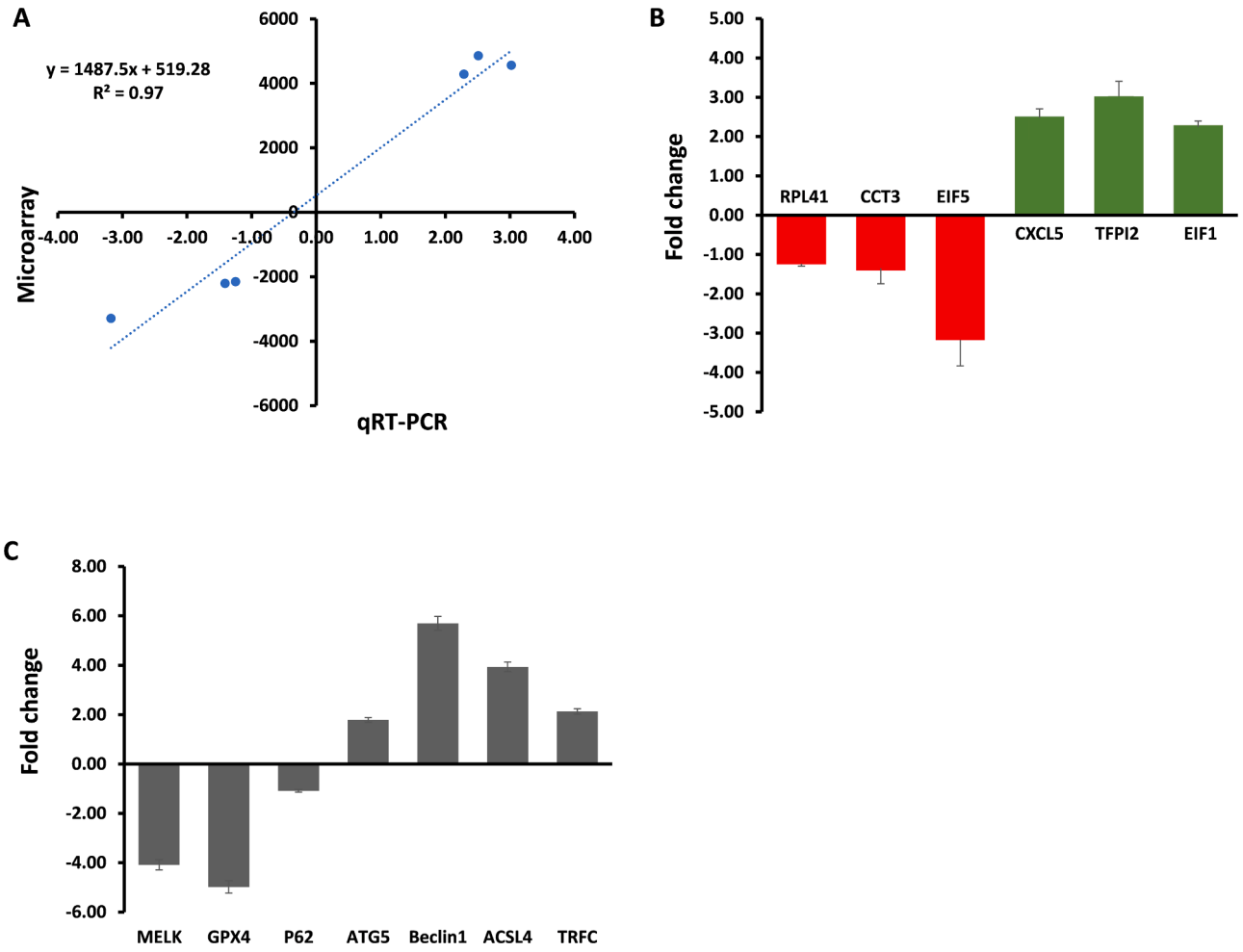

Fig. 4. Technical verification of microarray hybridization data using qRT-PCR analysis. (A) Linear regression and Pearson correlation coefficients of qRT-PCR (x-axis) and microarray data (y-axis) in A549 cells. (B) The expression level of top deregulated genes assessed in A549 cells treated with IC_{50} concentration of oleandrin compared to untreated cells. The x-axis represents the genes whereas the y-axis represents the fold change. These results reflect the mean values ± SD of three independent experiments. (C) The expression level of MELK, autophagy-related genes (Beclin1, ATG5 and P62), and ferroptosis-related genes (*GPX4, ACSL4,* and *TRFC*). The levels were assessed in A549 cells treated with IC_{50} concentration of oleandrin compared to untreated cells.

the second highest oleandrin response. Compared with untreated A549 cells, a total of 624 genes were deregulated upon treatment with oleandrin at IC_{50} (Supplementary Table S1). The results were further analysed using the Ingenuity Pathway Analyses software (IPA). These analyses revealed that various cellular functions and canonical pathways were affected by oleandrin, *e.g.*, cellular development, cellular growth and proliferation, cell death and survival, cellular movement, as well as cellular function and maintenance. Most notably, the analysis showed "cancer" as a top-affected disease (Fig. 3B). Subsequently, we further looked to the functions of DNA damage, apoptosis, and autophagy (Fig. 3C), to confirm these microarray-based findings using independent techniques. Comparing the oleandrin-treated A549 cells with untreated ones using IPA, the analysis of the upstream regulator revealed that A549 cells treated with oleandrin showed downregulated *MELK* expression (Fig. 3A), which is frequently overexpressed in NSCLC and causes metastasis and a worse survival prognosis (Ni et al., 2024; Tang et al., 2020; Zang et al., 2019). Therefore, we confirmed the downregulation of MELK expression using western blotting (Fig. 3D) and qRT-PCR (Fig. 4C) upon oleandrin treatment. Subsequently, we assessed the cellular functions of MELK, including mitosis, apoptosis, and cellular movement.

Oleandrin-induced gene expression alterations

The correlation between the determined fold changes of microarray hybridization and qRT-PCR data for the top deregulated genes (*CXCL5, TFPI2, EIF1, RPL41, CCT3,* and *EIF5)* was computed. The Pearson correlation coefficient was 0.97 ($p < 0.01$), indicating a high degree of agreement between these two methods (Fig. 4A, B).

Binding affinity of oleandrin to MELK in silico

The S score of the binding of oleandrin with the crystal structure of MELK protein (PDB: 5IH9) was –9.08 ± 0.13. Oleandrigenin (oleandrin aglycone) and NVS-MELK8a (the known inhibitor of MELK) showed less binding affinity to MELK than oleandrin with S scores of –7.39 ± 0.09, and –8.88 ± 0.09, respectively (Fig. 5). These results represent the mean values ± SD of three independent runs using MOE 2022.02.

Binding affinity of oleandrin in vitro

There was a strong binding between oleandrin and MELK recombinant protein as detected by the MST binding assay. The K_d value was 7.81 ± 0.98 μM (Fig. 6).

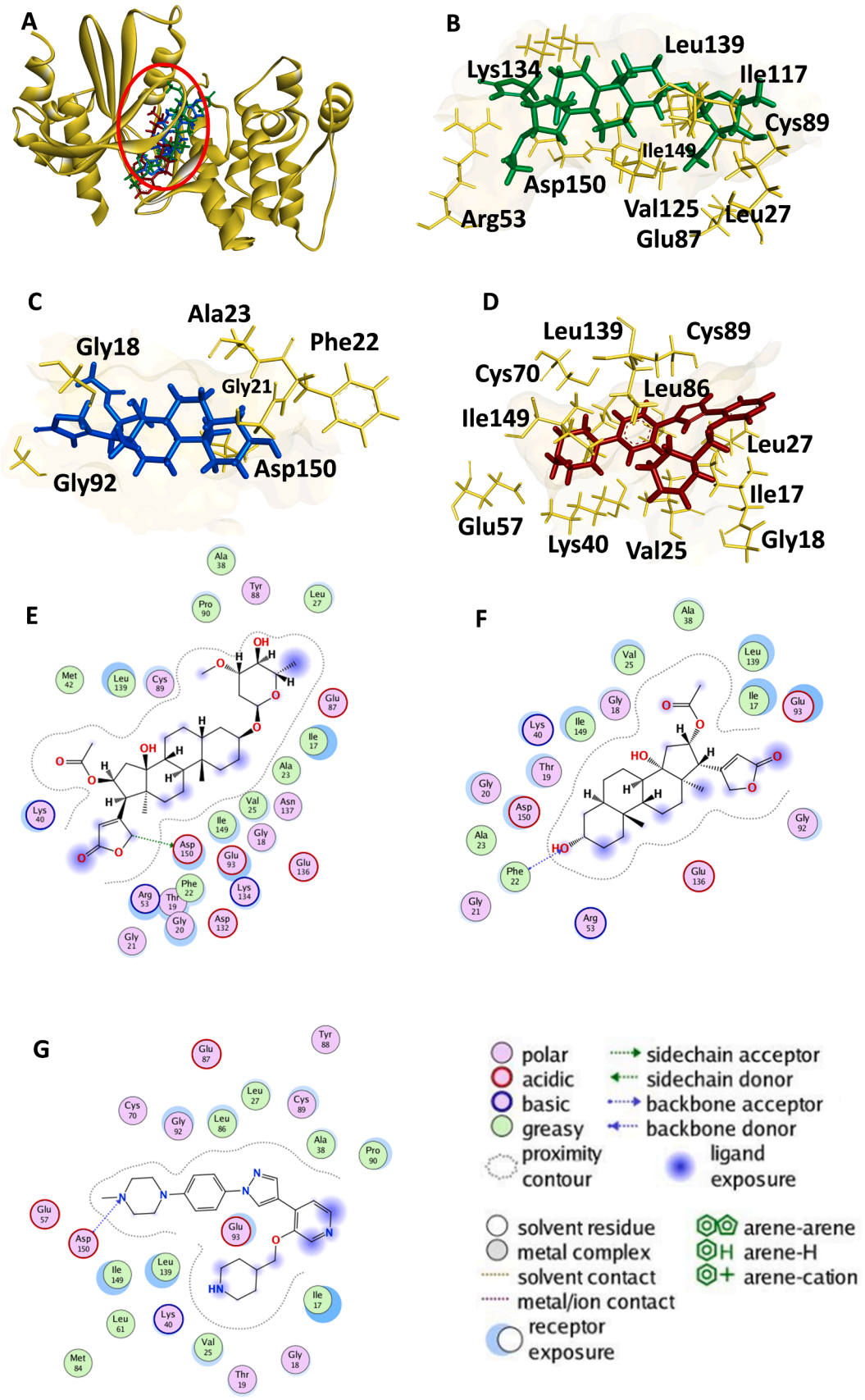

Fig. 5. MOE-molecular docking of ligands binding to MELK (PDB: 5IH9). (A) Binding of all candidates. Interactions of amino acid with (B) oleandrin (green), (C) oleandergenin (blue), and (D) the known inhibitor NVS-MELK8a (red). (E-G) are 2D views of (B-D), respectively. Images were created with the Discovery Studio visualizer.

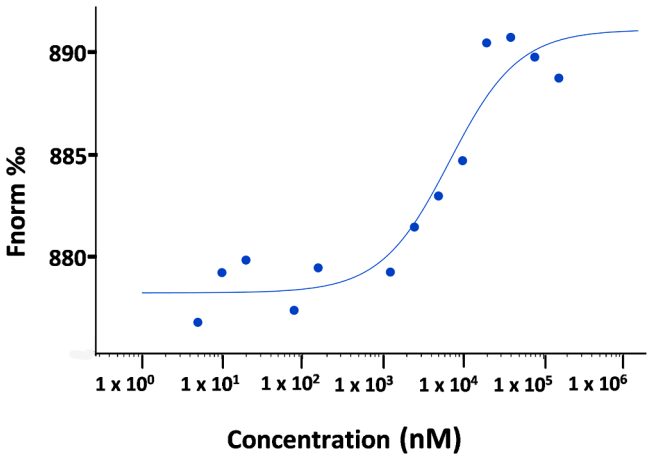

Fig. 6. Binding assay of oleandrin and MELK using MST. The x-axis represents oleandrin concentration, while the y-axis represents the percentage of Fnorm.

Microtubule network disruption and migration inhibition of A549 cells by oleandrin

We assumed that oleandrin might inhibit mitosis due to its inhibition of MELK. To test for mitosis inhibition, we examined the effect of oleandrin on microtubules. Microtubules are essential for the separation of chromosomes during mitosis. They are druggable targets in different types of cancers including lung, breast, and ovary tumors. Anti-tubulin agents such as taxanes and *Vinca* alkaloids are clinically established for the treatment of non-small cell lung cancer and many other tumor entities.

We investigated the effect of oleandrin on microtubules using U2OS cells stably transfected with an α-tubulin-GFP fusion cDNA construct. The cells were subjected to different concentrations of oleandrin equivalent to 0.5 × IC_{50}, IC_{50}, 2 × IC_{50}, and 4 × IC_{50}.

In the untreated control sample, the microtubules were spreading in the cytoplasm with appropriate networking and the nuclei had a normal morphology. Oleandrin-treated samples showed a similar morphology as paclitaxel-treated control cells specifically a condensation of microtubules and disintegration of nuclei (Fig. 7). The microtubules were shrunk, and they lost their extended network in a dose-dependent manner. Whereas vincristine-treated cells presented with decreased the expansion of microtubules at the margins keeping it surrounding the nucleus. The investigation of our data by IPA showed that the cellular movement was affected in oleandrin-treated cells. Considering that MELK is essential for cell migration, we investigated the effect of oleandrin on cell migratory capacity using an *in vitro* scratch assay with the A549 cell line. A concentration-dependent decrease in the wound-closure ability was observed with increasing concentrations of oleandrin (Fig. 8). The wound-closure percentage after 24 h incubation was 71.76 ± 2.35 %, 44.58 ± 5.35 %, 25.97 ± 3.49 %, 24.47 ± 3.58 %, and 16.09 ± 5.78 % in the untreated-control and samples treated with 0.5 × IC_{50}, IC_{50}, 2 × IC_{50}, or 4 × IC_{50}, respectively. After 48 h incubation, the values were 96.88 ± 5.41 %, 63.93 ± 2.49 %, 42.48 ± 4.98 %, 44.22 ± 6.08 %, and 27.35 ± 4.46 % for untreated-control, 0.5 × IC_{50}, IC_{50}, 2 × IC_{50} and 4 × IC_{50}, respectively (Fig. 8).

Oleandrin does not induce DNA damage

A previous report suggested that oleandrin induces DNA damage (Bao et al., 2016). Therefore, we performed single-cell electrophoresis (comet) assays under both neutral and alkaline conditions. Wild-type U2OS cells were treated with oleandrin concentrations equivalent to 0.5 × IC_{50}, IC_{50}, 2 × IC_{50}, and 4 × IC_{50}. While the positive control compound, t-BuOOH induced DNA breaks, the tail intensity upon oleandrin treatment was comparable to untreated control in both conditions indicating that oleandrin did not induce DNA-damage in U2OS cells (Fig. 9).

Oleandrin induces apoptosis, autophagy, and ferroptosis in A549 cells

It has been reported that both MELK inhibition and mitotic arrest can lead to apoptosis (Bhalla, 2003; Ibrado et al., 1998; Jordan, 2002; Tang et al., 2020). We measured induction of apoptosis by oleandrin using flow cytometry and SYTOX® AADvanced™ dead cell stain. After 48 h treatment, oleandrin induced apoptosis in A549 cells. Most prominently, treatment with 4 × IC_{50} concentration resulted in 17.7 % apoptotic cells compared with untreated cells (Fig. 10A and B). This result was further verified by western blot, which showed increased expression of cleaved caspase 3, indicating oleandrin induced apoptosis (Fig. 10C and D).

Flow cytometry was also used to detect autophagy. After 48 h incubation, the untreated control cells had less fluorescence signals than oleandrin-treated cells. The signal intensity decreased proportionately with increasing oleandrin concentrations. Remarkably, in higher concentrations, oleandrin induced autophagy more strongly than the positive control rapamycin (Fig. 11). We detected the expression levels of autophagy-related genes *BECN1* (Beclin1), *ATG5*, and *SQSTM1* (P62) using qRT-PCR. The former two genes were upregulated, whereas P62 was downregulated indicating induction of autophagy (Fig. 4C),

In order to detect ferroptosis, A549 cells were treated with the ferroptosis inhibitor ferrostatin-1 an hour before the treatment with oleandrin, followed by 48 h incubation. The IC_{50} of oleandrin increased from 7.20 ± 0.37 to 16.70 ± 0.24 nM upon inhibitor treatment, indicating that oleandrin induced a ferroptotic mode of cell death (Fig. 12). Using qRT-PCR, we detected the expression levels of ferroptosis-related genes *GPX4, ACSL4*, and *TRFC*, the latter two genes were upregulated whereas *GPX4* was highly downregulated indicating induction of ferroptosis (Fig. 4C).

Xenograft tumor animal assay

The efficacy and acute toxicity of oleandrin were tested *in vivo* in a A549 xenograft tumor zebrafish model. Cisplatin was used as positive control drug. As expected, it significantly inhibited the growth of the tumor in zebrafish (Fig. 13A). Oleandrin successfully reduced the tumor sizes in a dose-dependent manner in the three tested concentrations (Fig. 13B). These concentrations did not cause deaths in the zebrafish indicating reasonable safety (Fig. 13C).

ADMET analysis of oleandrin properties

We conducted an ADMET (absorption-distribution-metabolism-excretion-toxicology) analysis of oleandrin using ADMETlab 2.0 (https://admetmesh.scbdd.com). The results are shown in Supplementary Material S2. The prediction revealed that oleandrin has 9 hydrogen bond acceptors, two hydrogen bond donors, and 6 rotatable bonds. All these values and the other physicochemical properties were within the optimal range, except for the number of rigid bonds which was 33 (optimal is 0- 30). Oleandrin did not show any violation of the Lipinski's rule. The water solubility (log S) was –4.32. The partition coefficient logP was 2.38, indicating optimum partition. In general, the analysis predicted good absorption and distribution properties. Nevertheless, it showed median crossing of the blood-brain barrier. Oleandrin presented with a moderate clearance rate. Regarding rat oral acute toxicity, ADMETlab 2.0 generally classifies compounds into two categories: category 0 (low toxicity) and category 1 (high toxicity). Oleandrin reached a value of 0.96, indicating a high probability to rat oral acute toxicity. Regarding the FDA maximum recommended daily dose (FDAMDD), ADMETlab 2.0 has two categories: category 1 (FDAMDD+) and category 0 (FDAMDD–). A score of 0.95 for oleandrin indicated that it belonged to category 1.

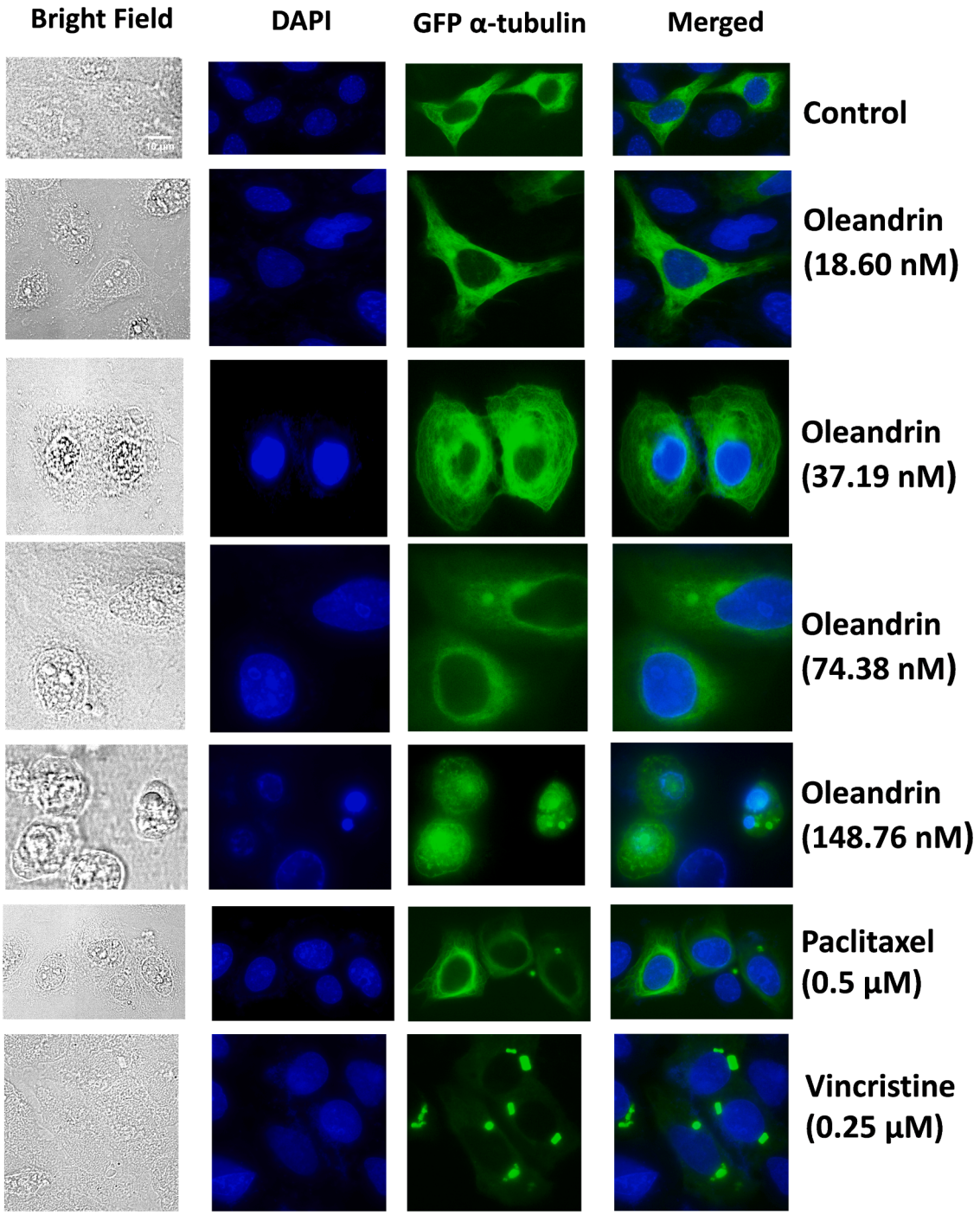

Fig. 7. Disruption of the microtubule network upon treatment with oleandrin in U2OS cells stably expressing GFP-α-tubulin protein. The cells were fixed with 4 % paraformaldehyde and stained with DAPI (blue stain in nuclei) after treatment for 24 h. Both paclitaxel (0.5 μM) and vincristine (0.25 μM) were used as controls as depolymerization inhibitor and polymerization inhibitor, respectively. An AF7000 widefield fluorescence microscope was used to capture the images (magnification: 40 ×; scale bar = 10 μm).

Discussion

Based on our recent results on a cold-water extract of *Nerium oleander*l. (Breastin) (Rashan et al., 2023), we investigated the tumor-supressing activity of oleandrin, one of the major constituents of *Nerium oleander* extract. In the current study, oleandrin was tested against 23 different cancer cell lines. Remarkably, it inhibited 16 cell lines at low nanomolar concentrations. The highest activity was in A549 non-small lung cancer cells. Therefore, we used this cell line for further investigation considering the need for less toxic and more effective drugs for this tumor entity.

The transcriptomics-based analyses of affected signaling pathways indicated that the treatment of A549 cells with oleandrin dysregulated the expression of number of genes. The technical validation of the microarray analysis was performed using qRT-PCR through testing three of the upregulated genes (*CXCL5, TFPI2,* and *EIF1*) besides three of the downregulated ones (*RPL41, CCT3,* and *EIF5*). The high calculated Pearson correlation coefficient was 0.97 ($p < 0.01$) signifying a substantial level of agreement between qRT-PCR and microarray hybridization analysis (Fig. 4).

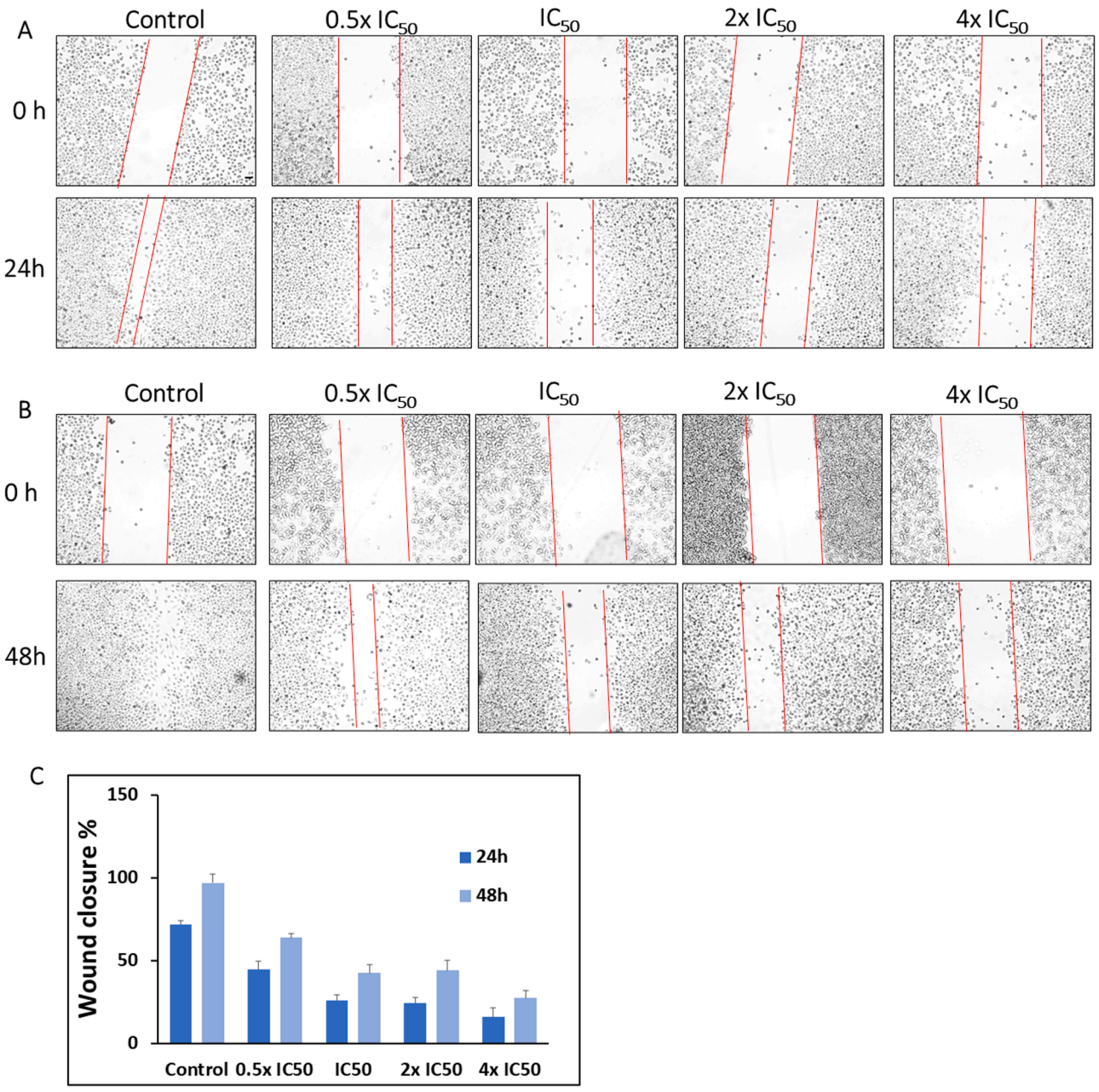

Fig. 8. Inhibition of A549 cells migration by different concentrations of oleandrin after exposure for (A) 24 h or (B) 48 h. (C) The bar chart indicates the percentage of wound closure (y-axis) after 24 h or 48 h treatment with oleandrin equivalent to 0.5 × IC_{50}, IC_{50}, 2 × IC_{50}, 4 × IC_{50} (x-axis). Data are presented as mean values ± SD of three independent experiments. The scale bar represents 100 μm.

These microarray hybridization data revealed that oleandrin down-regulated MELK in A549 cells. Even though the fact that MELK has been identified as an important oncogenic kinase, few MELK inhibitors have been developed to date. Therefore, we decided to investigate the MELK inhibitory activity of oleandrin in A549 cells in more detail. Consequently, we explored the cellular functions related to MELK, including cellular movement, mitotic progression, and programmed cell death (Speers et al., 2016).

For the examination of mitotic progression, we investigated the effect of our MELK inhibitor oleandrin on microtubules. As anticipated, oleandrin disturbed the microtubules extended network in a dose-dependent manner. The effect was similar to that exerted by the depolymerization inhibitor paclitaxel that was used as a control. The anti-mitotic effect of oleandrin could be attractive for further investigation in the future, because the number of available anti-mitotic drugs is limited for the treatment of NSCLC, and novel mitotic spindle inhibitors are needed. This finding aligned with our previous results on *Nerium oleander* extract, in which the depolymerization inhibitor activity of the extract has been demonstrated (Rashan et al., 2023). Our current results suggest that oleandrin was one of the components responsible for this activity. It is important to note that mitotic arrest also can lead to apoptosis (Blagosklonny, 2007). As tubulin inhibitors generally gained attention in cancer drug discovery, there are numerous microtubule inhibitors in preclinical studies and clinical trials (Edelman, 2009; Edelman and Shvartsbeyn, 2012; Gan et al., 2007; Hardin et al., 2017; Liu et al., 2022). On a related level, we tested cellular movement as it is highly affected by tubulin formation and MELK (Du et al., 2014; Xu et al., 2020), A decreased wound-closure ability was observed in a time- and concentration-dependent manner indicating that oleandrin inhibited cell migration. Previous studies reported that oleandrin inhibited

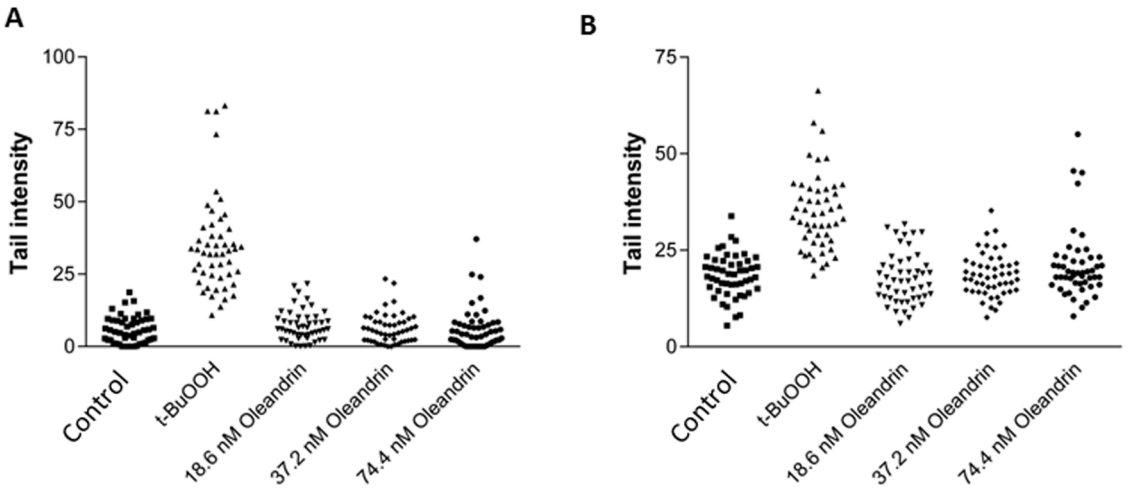

Fig. 9. Analysis of DNA single-strand breaks using the (A) alkaline comet assay and (B) neutral comet assay. The x-axis represents 50 U2OS wild-type cells which were analysed randomly for each of the experimental conditions including oleandrin-treated cells, un-treated cells (negative control) and t-BuOOH-treated cells (positive control), the y-axis represents the tail intensity.

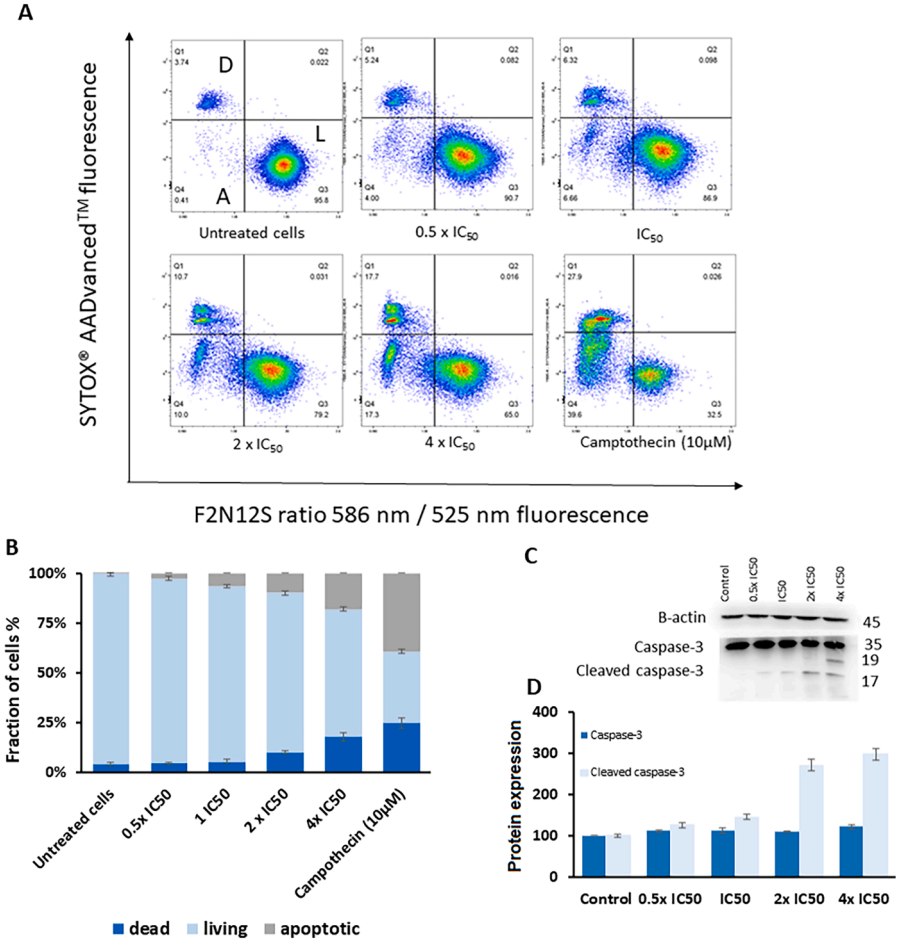

Fig. 10. Detection of apoptosis in oleandrin-treated A549 cells. (A) A549 cells treated with oleandrin equivalent to 0.5 × IC_{50}, IC_{50}, 2 × IC_{50}, and 4 × IC_{50} and the positive control camptothecin (10 µM). The cells were harvested after 48 h, stained according to the protocol. On a flow cytometer, samples were analyzed at 405 nm excitation for F2N12S using a 586/20 nm and a 525/45 nm bandpass filter. SYTOX® AADvanced™ dead cell stain was excited at 488 nm and detected using a bandpass filter of 695/40 nm. 50 thousand events were recorded. The samples were compared to untreated ones. *l*= living cells, *D* = dead cells *A* = apoptotic cells. The experiment was performed three times independently. (B) Quantification of living, dead, and apoptotic cells. The x-axis shows the tested concentrations of oleandrin whereas the y-axis shows the fraction of cells. (C) Detection of caspase-3 using western blotting. (D) Quantification of caspase-3 expression levels from Western blot, the x-axis shows the tested concentrations of oleandrin whereas the y-axis shows the expression of proteins after been normalized with negative control. All bar diagrams were obtained from the calculation of the mean value ± SD of three independent experiments performed at different time points.

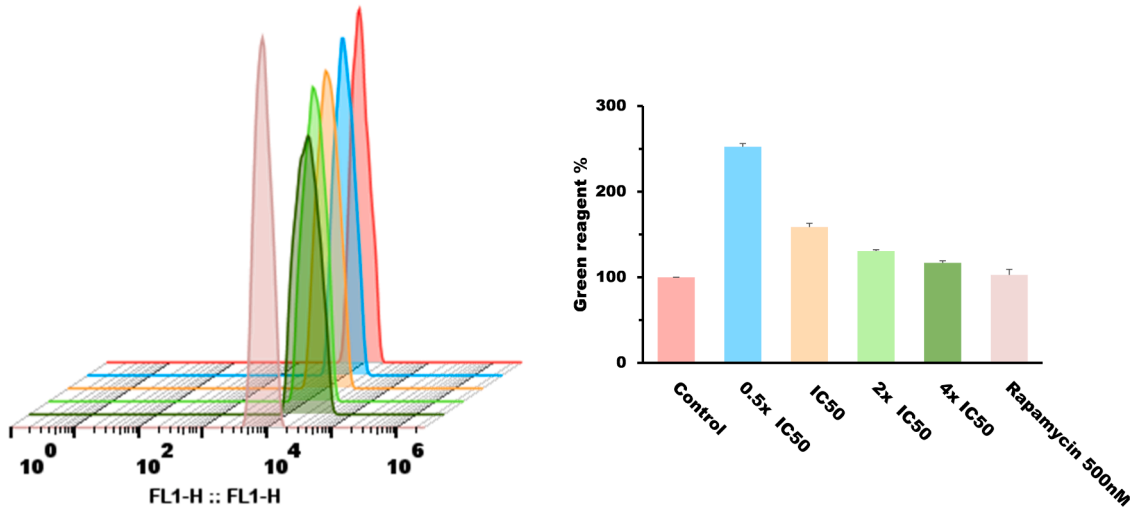

Fig. 11. Induction of autophagy in oleandrin-treated A549 cells. The cells were stained with green detection reagent after 48 h incubation. The fluorescence was measured using a flow cytometer at an excitation and an emission wavelength of 463 and 534 nm, respectively. The experiment was independently repeated three times to calculate the mean and SD values. The x-axis of the bar diagram axis shows the tested concentrations of oleandrin besides the negative control and the positive control rapamycin; however, the y-axis shows the fluorescence of the green reagent.

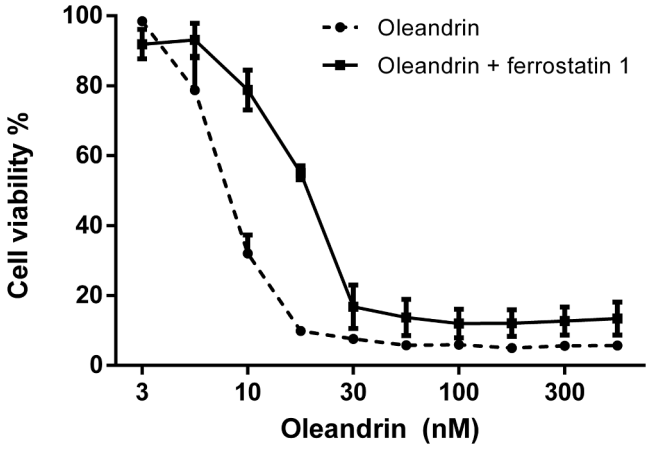

Fig. 12. Ferroptosis analysis of oleandrin-treated A549 cells using the resazurin reduction assay. The data represent the mean and SD of three independent experiments performed at different time points with six replicates each.

migration and invasion of U2OS and SaOS-2 osteosarcoma cells (Ma et al., 2015). Similarly, oleandrin was found to reduce cell migration in both human glioma (Garofalo et al., 2017) and Ishikawa endometrial adenocarcinoma cells (Secer Celik et al., 2023). Certainly, cell migration is particularly significant in pathological conditions, such as cancer invasion which is essential for cancer metastasis (Friedl and Wolf, 2010). The inhibition of cell migration has special importance in NSCLC, which is related to metastasis and poor prognosis.

Besides its effect on cellular movement and mitotic progression, MELK downregulation leads to programmed cell death. In the current investigation, we found that oleandrin induced different modes of programmed cell death in A549 cells, *i.e.*, apoptosis, autophagy, and ferroptosis. Oleandrin induced apoptosis in A549 cells in a dose-dependent manner as measured by the violet ratiometric membrane asymmetry probe/dead cell assay and western blotting. Oleandrin is a cardenolide steroidal glycoside that belongs to the family Apocynaceae from which 25 % of its isolated cardenolides had approved anticancer activity (Wen et al., 2016). Several other cardenolides from this family are known to effectively induce apoptosis in human tumor cells while having little negative effects on normal cells (Bloise et al., 2009; Martucciello et al., 2022; Rascón-Valenzuela et al., 2016; Verheye-Dua and Böhm, 2000; Wen et al., 2016). An example of the apoptotic cardenolides is digoxin (*Digitalis purpurea*), which has been involved in clinical trials to treat NSCLC, breast and prostate cancer. Similarly, the cardenolide UNBS1244 (*Calotropis procera*) and its semisynthetic derivative UNBS-1450 had been clinically trailed after its approved efficacy in A549, NCI-H727, A427, and CAL-12T cell types of NSCLC (Wen et al., 2016). Correspondingly, ouabain (from *Strophanthus gratus*) together with several other cardenolides had induced apoptosis if tested in 143B osteosarcoma cells (Delebinski et al., 2015). Our experimental data showed that oleandrin exerted anticancer effects by efficiently inhibiting the proliferation of A549 lung cancer cells without causing considerable harm to healthy cells, including normal human lung cells MRC-5, human PBMCs and normal murine hepatocytes AML-12, suggesting that oleandrin could have an acceptable safety profile.

Additionally, it has been reported that the inhibition of MELK induces apoptosis mediated by caspase-3. Here, the apoptotic effect of oleandrin may be comparable to the action of the known MELK inhibitor, OTSSP167 (Pitner et al., 2017; Tang et al., 2020). Moreover, oleandrin has also been reported to induce caspase-3-dependent apoptosis in PC-3 prostatic cancer cells, thereby increasing the cellular sensitivity to radiotherapy (Nasu et al., 2002).

Furthermore, oleandrin significantly induced autophagy in a dose-dependent manner after 48 h incubation (Fig. 11). Unexpectedly, autophagy induced by oleandrin dose-dependently decreased, while apoptosis induction increased. It can be speculated that various modes of programmed cell death occur simultaneously and that a switch from autophagy at low concentrations to apoptosis at higher concentrations of oleandrin took place in A549 cells. For additional verification, we tested the expression level of autophagy-related genes *BECN1, ATG5,* and *SQSTM1* using qRT-PCR. Both *BECN1* and *ATG5* were highly up-regulated whereas there was a down-regulation P62 indicating induction of autophagy (Fig. 4.C). To the best of our knowledge, it is the first time to demonstrate oleandrin autophagy induction in A549 lung cancers. Autophagy by oleandrin has been recently reported human PANC-1 pancreatic cancer cells (Newman et al., 2007).

Interestingly, oleandrin also induced ferroptosis besides apoptosis and autophagy in A549 cells. Using the ferroptosis inhibitor ferrostatin-1, the IC_{50} value of oleandrin moderately increased from 6.98 ± 1.28 nM to 16.70 ± 0.24 nM indicating that ferroptosis was operative. We confirmed this result with testing the expression levels of three ferroptosis-related genes. Oleandrin-treated cells showed up-regulation

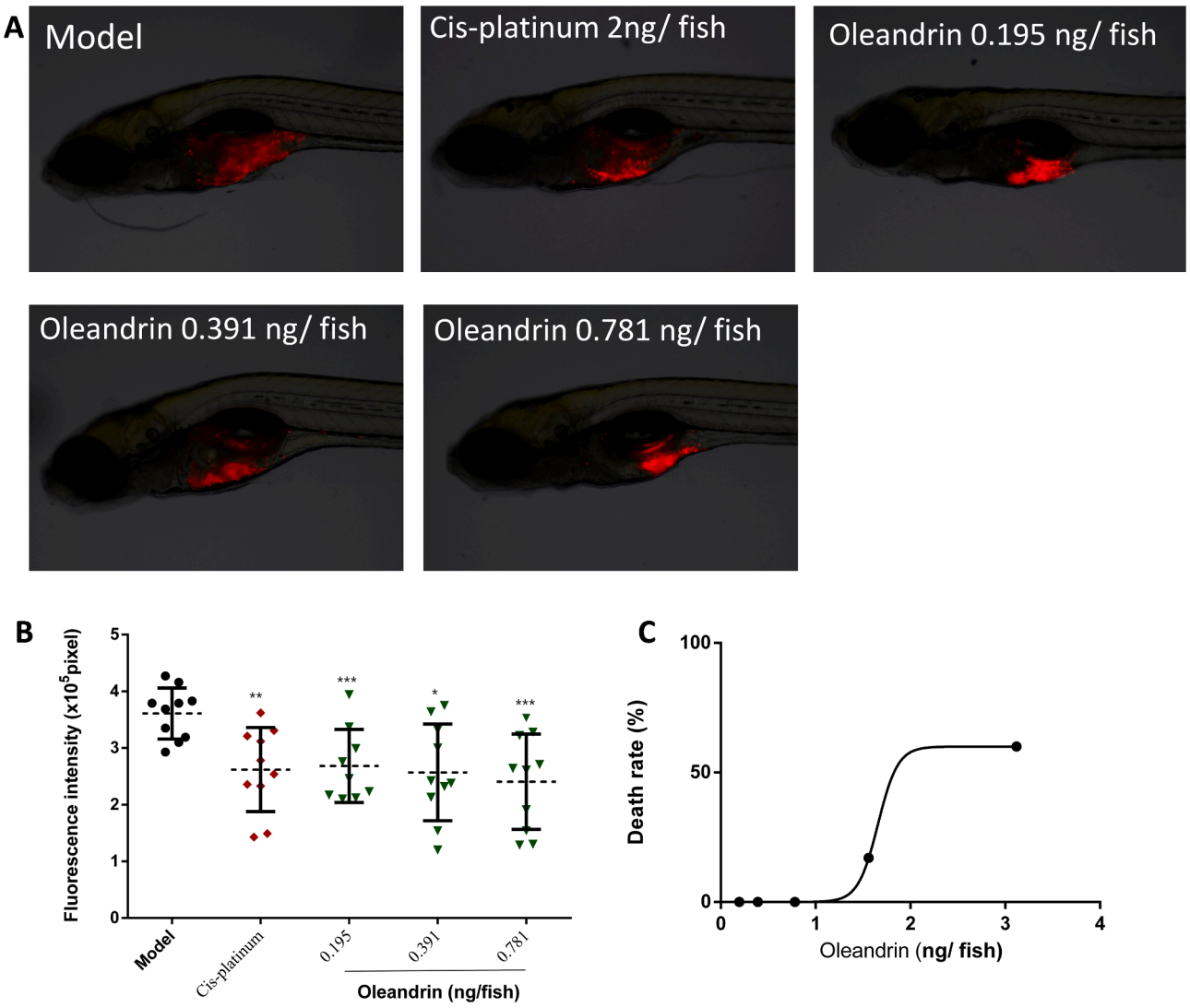

Fig. 13. (A) A549 xenograft observation in zebrafish treated with indicated doses of oleandrin and the positive control cis-platinum. The red fluorescence reflects A549 tumor mass. Images were captured at 60× magnification (scale bars = 100 μm) (B) Statistical data of red fluorescence intensity (y-axis) for A549 cells in response to treatment with oleandrin and positive control (x-axis). Using unpaired 2-tailed student's T-test, the values were presented as the mean ± SD. *: $p < 0.05$, **: $p < 0.01$ and ***: $p < 0.001$ compared to the model. (C) Acute toxicity expressed as death rate (%) ($n = 30$).

of *ACSL4* and *TRFC* whereas GPX4 was highly downregulated indicating induction of ferroptosis (Fig. 4.C). These results correspond with the signaling pathway analysis of our transcriptomic mRNA expression data, where we found that oleandrin induced ferroptosis. This is the first time to report the potential of oleandrin to induce ferroptosis.

After the establishment of the Trans-NIH Zebrafish Coordinating Committee at the National Institutes of Health in 1997 (Grunwald and Eisen, 2002), zebrafish (*Danio rerio*) had been widely used as a model in studying human cancer biology and metastasis. This is due to histopathological similarities between human and zebrafish tumors, and the ease of genetic modification. The larval zebrafish is an ideal *in vivo* model for the injection of malignant cells without the risk of rejection since it lacks adaptive immunity. In addition, the transparency of the animal allows monitoring and imaging of the tumor (Amatruda et al., 2002; Astell and Sieger, 2020). Here, oleandrin significantly reduced the growth of A549 tumors, showing dose-dependent inhibition at dosages of 0.195, 0.391 and 0.781 ng. Neither side effects nor deaths were observed (Fig. 13).

Oleandrigenin is the first metabolite that appears during the degradation of oleandrin in the body. In the first pass of the drug in the mice liver, oleandrin content is >60 %, whereas oleandrigenin is 28 % (Zhai et al., 2022). Because oleandrigenin is a bioactive metabolite, we performed molecular docking of both oleandrigenin and oleandrin to see whether or not these compounds may bind with MELK. We used NVS-MELK8a rather than OTSSP167 as a control inhibitor of MELK because of its selectivity (62,63). We docked these three molecules to the ligand binding site using MOE 2022.02. Our analysis indeed showed the potential of oleandrin to bind to the ligand binding pocket in the crystal structure of the MELK protein. Interestingly, the S-value for oleandrin was –9.08 ± 0.13 kcal/mol which is lower than that of NVS-MELK8a (–7.39 ± 0.09 kcal/mol), indicating that oleandrin had higher binding affinity to the ligand binding pocket than the inhibitor NVS-MELK8a itself (Fig. 5). Oleandrigenin was also bound to the ligand binding pocket of MELK but with less affinity than oleandrin. The weaker binding affinity of oleandrogenin as degradation product of the parental compound oleandrin indicates that the metabolization process within the body leads to decreased rather than increased bioactivities. We further assessed the binding between oleandrin and MELK using MST, a biophysical method that measures the strength of molecular interactions. As anticipated, oleandrin had strongly bound to MELK labelled protein with K_d 7.81 ± 0.98 μM (Fig. 6). This relatively high K_d value compared to IC_{50} suggests that the inhibition of MELK might not

the exclusive mechanism for oleandrin. Oleandrin also affected other cellular mechanisms such as inducing DNA damage responses in lung cancer cells by suppressing the expression of Rad51 (Bao et al., 2016). It also inhibited the invasion of breast cancer cells MDA-MB-231 and RT-R-MDA-MB-231 by suppressing the STAT-3 signalling pathway (Ko et al., 2018).

MELK is highly expressed in NSCLC (Tang et al., 2020; Zang et al., 2019). Important studies demonstrated that MELK is preferentially expressed in cancer cells rather than the vital organs such as the heart, liver, lung and kidney (Ganguly et al., 2014; Lin et al., 2007; McDonald et al., 2020; Touré et al., 2016). MELK exclusively binds to the oncogenic transcription factors c-Jun and FoxM1 forming a heterotrimeric complex in cancer stem cells. However, it does not bind to normal progenitor and stem cells (Gu et al., 2013; Joshi et al., 2013). Therefore, the development of selective MELK inhibitors could be highly valuable in the treatment of cancers in these organs with minimum side effects in normal tissues.

The analysis of the absorption-distribution-metabolism-excretion-toxicology (ADMET) properties indicated that oleandrin might potentially exert some toxic activity. However, our data revealed that oleandrin has a reasonable safety profile if tested against MRC-5 normal lung fibroblasts with a good selectivity index of 31.56. Moreover, oleandrin did not affect PBMC and normal hepatocytes AML-12 in the investigated concentration range. Still, oleandrin may cause side effects at higher concentrations since preclinical *in vivo* trials on beagles showed that a dose exceeding 6.9 μg/kg caused cardiac toxicity, while 4.6 μg/kg had no negative effects (Fossum et al., 2024). Even though, many of the clinically established anticancer drugs were derived from poisonous plants such as paclitaxel from *Taxus* spp., as well as vincristine and vinblastine from *Catharanthus roseus,* and others. This fact should motivate further investigations on this highly promising molecule.

Cardiac glycosides are known for their toxicity, especially cardiotoxicity. In a clinical phase 1 trial with Breastin, rather mild and tolerable side effects were observed in patients which were compatible with those seen in mouse experiments (Fiebig et al., 2008). Another aqueous *N. oleander* extract (Anvirzel) also only showed mild toxicities in a clinical phase 1 trial with tumor patients, *e.g.*, fatigue, nausea, vomiting, and dyspnea (Mekhail et al., 2006). A serious problem represents self-medication with oleander leaves (Bavunoğlu et al., 2016; Carfora et al., 2021). Side effects of *Nerium oleander* and oleandrin include the gastrointestinal system (nausea and vomiting, excess salivation, abdominal pain, diarrhea), heart (arrhythmia, hypotension), and central nervous system (drowsiness, muscle tremors, seizures, collapse, and coma) (Guru et al., 2021; Zhai et al., 2022). Lethal oleander intoxications occurred more frequently in children than in adults (Langford and Boor, 1996). Although the preliminary data with Breastin and Anvirzel did not speak for severe and life-threatening side effects, it is wise to be cautious. If oleandrin or standardized *Nerium oleander* would ever reach the clinics, close monitoring of side effects is necessary. Self-medication is strongly discouraged as it is for any other established anticancer drug as well.

Conclusion

In this study, we reported oleandrin for the first time as MELK inhibitor in A549 cells. We suggested that oleandrin could be valuable in NSCLC therapy research in the future. However, additional in-depth research is necessary to characterize its safety profile and its suitability for future development.

CRediT authorship contribution statement

Ejlal A. Omer: Writing – original draft, Visualization, Software, Methodology, Investigation, Formal analysis, Conceptualization. **Min Zhou:** Methodology. **Wynand P. Roos:** Writing – review & editing, Methodology. **Luay J. Rashan:** Methodology. **Heinz-Herbert Fiebig:** Methodology. **Sabine M. Klauck:** Writing – review & editing, Methodology. **Letian Shan:** Methodology. **Thomas Efferth:** Writing – review & editing, Supervision, Conceptualization.

Declaration of competing interest

The other authors do not have a conflict of interest.

Acknowledgement

We gratefully acknowledge the German Academic Exchange Service (DAAD) for a Ph.D. stipend to E.A. O. We also acknowledge the Microarray Core Facility, German Cancer Research Center (DKFZ, Heidelberg, Germany) for providing excellent mRNA-based Expression Profiling services. We are also thankful to the Flow Cytometry Core Facility at the Institute of Molecular Biology (IMB, Mainz, Germany) for providing training and technical assistance for the usage of Novocyte Quanteon (Agilent) for detection of apoptosis.

Supplementary materials

Supplementary material associated with this article can be found, in the online version, at doi:10.1016/j.phymed.2025.157173.

References

Alachkar, H., Mutonga, M., Metzeler, K., Fulton, N., Malnassy, G., Herold, T., Spiekermann, K., Bohlander, S., Hiddemann, W., Matsuo, Y., Stock, W., Nakamura, Y., 2014. Preclinical efficacy of maternal embryonic leucine-zipper kinase (MELK) inhibition in acute myeloid leukemia. Oncotarget. 5. https://doi.org/10.18632/oncotarget.2642.

Amatruda, J.F., Shepard, J.L., Stern, H.M., Zon, L.I., 2002. Zebrafish as a cancer model system. Cancer Cell 1, 229–231. https://doi.org/10.1016/s1535-6108(02)00052-1.

Astell, K.R., Sieger, D., 2020. Zebrafish *In vivo* models of cancer and metastasis. Cold. Spring. Harb. Perspect. Med. 10, a037077. https://doi.org/10.1101/cshperspect.a037077.

Bao, Z., Tian, B., Wang, X., Feng, H., Liang, Y., Chen, Z., Li, W., Shen, H., Ying, S., 2016. Oleandrin induces DNA damage responses in cancer cells by suppressing the expression of Rad51. Oncotarget. 7, 59572–59579. https://doi.org/10.18632/oncotarget.10726.

Bavunoğlu, I., Balta, M., Türkmen, Z., 2016. Oleander poisoning as an example of self-medication attempt. Balkan. Med. J. 33, 559–562. https://doi.org/10.5152/balkanmedj.2016.150307.

Bhalla, K.N., 2003. Microtubule-targeted anticancer agents and apoptosis. Oncogene 22, 9075–9086. https://doi.org/10.1038/sj.onc.1207233.

Bhuvaneshwari, L., Arthy, E., Anitha, C., Dhanabalan, K., Meena, M., 2007. Phytochemical analysis & antibacterial activity of nerium oleander. Anc. Sci. Life 26, 24.

Blagosklonny, M.V., 2007. Mitotic arrest and cell fate: why and how Mitotic inhibition of transcription drives mutually exclusive events. Cell Cycle 6, 70–74. https://doi.org/10.4161/cc.6.1.3682.

Bloise, E., Braca, A., De Tommasi, N., Belisario, M.A., 2009. Pro-apoptotic and cytostatic activity of naturally occurring cardenolides. Cancer Chemother Pharmacol. 64, 793–802. https://doi.org/10.1007/s00280-009-0929-5.

Boulos, J.C., Chatterjee, M., Shan, L., Efferth, T., 2023a. Silico, *In Vitro*, and *In Vivo* investigations on adapalene as repurposed third generation retinoid against multiple myeloma and leukemia. Cancers. (Basel) 15, 4136. https://doi.org/10.3390/cancers15164136.

Boulos, J.C., Omer, E.A., Rigano, D., Formisano, C., Chatterjee, M., Leich, E., Klauck, S. M., Shan, L., Efferth, T., 2023b. Cynaropicrin disrupts tubulin and c-myc-related signaling and induces parthanatos-type cell death in multiple myeloma. Acta Pharmacol. Sin. 44, 2265–2281. https://doi.org/10.1038/s41401-023-01117-3.

Carfora, A., Petrella, R., Borriello, R., Aventaggiato, L., Gagliano-Candela, R., Campobasso, C.P., 2021. Fatal poisoning by ingestion of a self-prepared oleander leaf infusion. Forensic Sci. Med. Pathol. 17, 120–125. https://doi.org/10.1007/s12024-020-00338-w.

Chen, S., Zhou, Q., Guo, Z., Wang, Y., Wang, L., Liu, X., Lu, M., Ju, L., Xiao, Y., Wang, X., 2020. Inhibition of MELK produces potential anti-tumour effects in bladder cancer by inducing G1/S cell cycle arrest via the ATM/CHK2/p53 pathway. J. Cell Mol. Med. 24, 1804–1821. https://doi.org/10.1111/jcmm.14878.

Choi, S., Ku, J.-L., 2011. Resistance of colorectal cancer cells to radiation and 5-FU is associated with MELK expression. Biochem. Biophys. Res. Commun. 412, 207–213. https://doi.org/10.1016/j.bbrc.2011.07.060.

de Jager, V.D., Timens, W., Bayle, A., Botling, J., Brcic, L., Büttner, R., Fernandes, M.G. O., Havel, L., Hochmair, M.J., Hofman, P., Janssens, A., Johansson, M., Kempen, L. van, Kern, I., Lopez-Rios, F., Lüchtenborg, M., Machado, J.C., Mohorcic, K., Paz-Ares, L., Popat, S., Ryška, A., Taniere, P., Wolf, J., Schuuring, E., Wekken, A.J., van der, 2024. Developments in predictive biomarker testing and targeted therapy in

advanced stage non-small cell lung cancer and their application across European countries. The Lancet Region. Health – Europe 38. https://doi.org/10.1016/j.lanepe.2024.100838.
Delebinski, C.I., Georgi, S., Kleinsimon, S., Twardziok, M., Kopp, B., Melzig, M.F., Seifert, G., 2015. Analysis of proliferation and apoptotic induction by 20 steroid glycosides in 143B osteosarcoma cells *in vitro*. Cell Prolif. 48, 600–610. https://doi.org/10.1111/cpr.12208.
Dengler, W.A., Schulte, J., Berger, D.P., Mertelsmann, R., Fiebig, H.H., 1995. Development of a propidium iodide fluorescence assay for proliferation and cytotoxicity assays. Anticancer Drugs 6, 522–532. https://doi.org/10.1097/00001813-199508000-00005.
Dominguez-Brauer, C., Thu, K.L., Mason, J.M., Blaser, H., Bray, M.R., Mak, T.W., 2015. Targeting mitosis in cancer: emerging strategies. Mol. Cell 60, 524–536. https://doi.org/10.1016/j.molcel.2015.11.006.
Du, T., Qu, Y., Li, J., Li, H., Su, L., Zhou, Q., Yan, M., Li, C., Zhu, Z., Liu, B., 2014. Maternal embryonic leucine zipper kinase enhances gastric cancer progression via the FAK/Paxillin pathway. Mol. Cancer 13, 100. https://doi.org/10.1186/1476-4598-13-100.
Duhig, E.E., Dettrick, A., Godbolt, D.B., Pauli, J., van Zwieten, A., Hansen, A.R., Yang, I. A., Fong, K.M., Clarke, B.E., Bowman, R.V., 2015. Mitosis trumps T stage and proposed International Association for the Study of Lung Cancer/American Thoracic Society/European Respiratory Society Classification for prognostic value in resected stage 1 Lung adenocarcinoma. J. Thorac. Oncol. 10, 673–681. https://doi.org/10.1097/JTO.0000000000000446.
Dunn, D.E., He, D.N., Yang, P., Johansen, M., Newman, R.A., Lo, D.C., 2011. *In vitro* and *in vivo* neuroprotective activity of the cardiac glycoside oleandrin from Nerium oleander in brain slice-based stroke models. J. Neurochem. 119, 805–814. https://doi.org/10.1111/j.1471-4159.2011.07439.x.
Edelman, M.J., 2009. Novel taxane formulations and microtubule-binding agents in non–Small-cell lung cancer. Clin. Lung Cancer 10, S30–S34. https://doi.org/10.3816/CLC.2009.s.005.
Edelman, M.J., Shvartsbeyn, M., 2012. Epothilones in development for non–Small-cell lung cancer: novel anti-tubulin agents with the potential to overcome taxane resistance. Clin. Lung Cancer 13, 171–180. https://doi.org/10.1016/j.cllc.2011.02.005.
El-Akhal, F., Guemmouh, R., Ez Zoubi, Y., El Ouali Lalami, A., 2015. Larvicidal activity of *nerium oleander* against larvae West Nile vector Mosquito *culex pipiens* (Diptera: culicidae). J. Parasitol. Res. 2015, e943060. https://doi.org/10.1155/2015/943060.
Ettinger, D.S., Wood, D.E., Aisner, D.L., Akerley, W., Bauman, J.R., Bharat, A., Bruno, D. S., Chang, J.Y., Chirieac, L.R., D'Amico, T.A., DeCamp, M., Dilling, T.J., Dowell, J., Gettinger, S., Grotz, T.E., Gubens, M.A., Hegde, A., Lackner, R.P., Lanuti, M., Lin, J., Loo, B.W., Lovly, C.M., Maldonado, F., Massarelli, E., Morgensztern, D., Ng, T., Otterson, G.A., Pacheco, J.M., Patel, S.P., Riely, G.J., Riess, J., Schild, S.E., Shapiro, T.A., Singh, A.P., Stevenson, J., Tam, A., Tanvetyanon, T., Yanagawa, J., Yang, S.C., Yau, E., Gregory, K., Hughes, M., 2022. Non–Small cell Lung Cancer, Version 3.2022, NCCN Clinical Practice Guidelines in Oncology. J. Natl. Comprehens. Cancer Netw. 20, 497–530. https://doi.org/10.6004/jnccn.2022.0025.
Fakoorziba, M.R., Moemenbellah-Fard, M.D., Azizi, K., Mokhtari, F., 2015. Mosquitocidal efficacy of medicinal plant, *nerium oleander* (Apocynaceae), leaf and flower extracts against malaria vector, *Anopheles stephensi* Liston (Diptera: culicidae) larvae. Asian Pac. J. Trop. Dis. 5, 33–37. https://doi.org/10.1016/S2222-1808(14)60623-X.
Fiebig, H.H., Berger, D.P., Dengler, W.A., Wallbrecher, E., Winterhalter, B.R., 1992. Combined In Vitro/In Vivo test procedure with Human tumor xenografts for new drug development. https://doi.org/10.1159/000421298.
Fiebig, H.-H., Rashan, J.J., Rashan, F.J., 2008. Therapeutic use of an extract from the leaves of nerium oleander. EP1976542A1.
Fossum, T.W., Newman, R.A., Matos, J.R., 2024. Preliminary investigation of the safe dose of oleandrin when administered orally to Beagles. J. Am. Vet. Med. Assoc. 1, 1–7. https://doi.org/10.2460/javma.23.11.0651.
Friedl, P., Wolf, K., 2010. Plasticity of cell migration: a multiscale tuning model. J. Cell Biol. 188, 11–19. https://doi.org/10.1083/jcb.200909003.
Gan, P.P., Pasquier, E., Kavallaris, M., 2007. Class III β-tubulin mediates sensitivity to chemotherapeutic drugs in non–Small cell lung cancer. Cancer Res. 67, 9356–9363. https://doi.org/10.1158/0008-5472.CAN-07-0509.
Ganguly, R., Hong, C.S., Smith, L.G.F., Kornblum, H.I., Nakano, I., 2014. Maternal embryonic leucine zipper kinase: key kinase for stem cell phenotype in glioma and other cancers. Mol. Cancer Ther. 13, 1393–1398. https://doi.org/10.1158/1535-7163.MCT-13-0764.
Ganguly, R., Mohyeldin, A., Thiel, J., Kornblum, H.I., Beullens, M., Nakano, I., 2015. MELK—A conserved kinase: functions, signaling, cancer, and controversy. Clin. Transl. Med. 4, 11. https://doi.org/10.1186/s40169-014-0045-y.
Garofalo, S., Grimaldi, A., Chece, G., Porzia, A., Morrone, S., Mainiero, F., D'Alessandro, G., Esposito, V., Cortese, B., Angelantonio, S.D., Trettel, F., Limatola, C., 2017. The glycoside oleandrin reduces glioma growth with direct and indirect effects on tumor cells. J. Neurosci. 37, 3926–3939. https://doi.org/10.1523/JNEUROSCI.2296-16.2017.
Gayathri, V., Ananthi, S., Chandronitha, C., Ramakrishnan, G., Lakshmisundaram, R., Vasanthi, H.R., 2011. Cardioprotective effect of Nerium oleander flower against isoproterenol-induced myocardial oxidative stress in experimental rats. J. Cardiovasc. Pharmacol. Ther. 16, 96–104. https://doi.org/10.1177/1074248410381759.
Grada, A., Otero-Vinas, M., Prieto-Castrillo, F., Obagi, Z., Falanga, V., 2017. Research techniques made simple: analysis of collective cell migration using the wound healing assay. J. Invest. Dermatol. 137, e11–e16. https://doi.org/10.1016/j.jid.2016.11.020.
Gray, D., Jubb, A.M., Hogue, D., Dowd, P., Kljavin, N., Yi, S., Bai, W., Frantz, G., Zhang, Z., Koeppen, H., de Sauvage, F.J., Davis, D.P., 2005. Maternal embryonic leucine zipper kinase/murine protein serine-threonine kinase 38 is a promising therapeutic target for multiple cancers. Cancer Res. 65, 9751–9761. https://doi.org/10.1158/0008-5472.CAN-04-4531.
Grunwald, D.J., Eisen, J.S., 2002. Headwaters of the zebrafish – emergence of a new model vertebrate. Nat. Rev. Genet. 3, 717–724. https://doi.org/10.1038/nrg892.
Gu, C., Banasavadi-Siddegowda, Y.K., Joshi, K., Nakamura, Y., Kurt, H., Gupta, S., Nakano, I., 2013. Tumor-specific activation of the c-JUN/MELK pathway regulates glioma stem cell growth in a p53-dependent manner. Stem Cells (1981) 31, 870–881. https://doi.org/10.1002/stem.1322.
Guru, S., Behera, A., Barik, S., Hansdah, U., Mohanty, C.R., Sahoo, S., 2021. Severe oleander poisoning presenting with hyperkalaemia and unusual electrocardiographic changes. Eur. J. Case Rep. Intern. Med. 8, 003044. https://doi.org/10.12890/2021_003044.
Hardin, C., Shum, E., Singh, A., Perez-Soler, R., Cheng, H., 2017. Emerging treatment using tubulin inhibitors in advanced non-small cell lung cancer. Expert. Opin. PharmacOther 18, 701–716. https://doi.org/10.1080/14656566.2017.1316374.
Ibrado, A.M., Kim, C.N., Bhalla, K., 1998. Temporal relationship of CDK1 activation and mitotic arrest to cytosolic accumulation of cytochrome C and caspase-3 activity during Taxol-induced apoptosis of human AML HL-60 cells. Leukemia 12, 1930–1936. https://doi.org/10.1038/sj.leu.2401218.
Inoue, H., Kato, T., Olugbile, S., Tamura, K., Chung, S., Miyamoto, T., Matsuo, Y., Salgia, R., Nakamura, Y., Park, J.-H., 2016. Effective growth-suppressive activity of maternal embryonic leucine-zipper kinase (MELK) inhibitor against small cell lung cancer. Oncotarget. 7, 13621–13633. https://doi.org/10.18632/oncotarget.7297.
Jordan, M.A., 2002. Mechanism of action of antitumor drugs that interact with microtubules and tubulin. Curr. Med. Chem. AntiCancer Agents 2, 1–17. https://doi.org/10.2174/1568011023354290.
Joshi, K., Banasavadi-Siddegowda, Y., Mo, X., Kim, S.-H., Mao, P., Kig, C., Nardini, D., Sobol, R.W., Chow, L.M.L., Kornblum, H.I., Waclaw, R., Beullens, M., Nakano, I., 2013. MELK-dependent FOXM1 phosphorylation is essential for proliferation of glioma stem cells. Stem Cells (1981) 31, 1051–1063. https://doi.org/10.1002/stem.1358.
Kim, S.-H., Joshi, K., Ezhilarasan, R., Myers, T.R., Siu, J., Gu, C., Nakano-Okuno, M., Taylor, D., Minata, M., Sulman, E.P., Lee, J., Bhat, K.P.L., Salcini, A.E., Nakano, I., 2015. EZH2 protects glioma stem cells from radiation-induced cell death in a MELK/FOXM1-dependent manner. Stem Cell Reports. 4, 226–238. https://doi.org/10.1016/j.stemcr.2014.12.006.
Ko, Y.S., Rugira, T., Jin, H., Park, S.W., Kim, H.J., 2018. Oleandrin and its derivative odoroside A, both cardiac glycosides, exhibit anticancer effects by inhibiting invasion via suppressing the STAT-3 signaling pathway. Int. J. Mol. Sci. 19, 3350. https://doi.org/10.3390/ijms19113350.
Kohler, R.S., Kettelhack, H., Knipprath-Mészaros, A.M., Fedier, A., Schoetzau, A., Jacob, F., Heinzelmann-Schwarz, V., 2017. MELK expression in ovarian cancer correlates with poor outcome and its inhibition by OTSSP167 abrogates proliferation and viability of ovarian cancer cells. Gynecol. Oncol. 145, 159–166. https://doi.org/10.1016/j.ygyno.2017.02.016.
Langford, S.D., Boor, P.J., 1996. Oleander toxicity: an examination of human and animal toxic exposures. Toxicology. 109, 1–13. https://doi.org/10.1016/0300-483x(95)03296-r.
Lans, C., 2007. Ethnomedicines used in Trinidad and Tobago for reproductive problems. J. Ethnobiol. Ethnomed. 3, 13. https://doi.org/10.1186/1746-4269-3-13.
Lin, M.-L., Park, J.-H., Nishidate, T., Nakamura, Y., Katagiri, T., 2007. Involvement of maternal embryonic leucine zipper kinase (MELK) in mammary carcinogenesis through interaction with Bcl-G, a pro-apoptotic member of the Bcl-2 family. Breast Cancer Res. 9, R17. https://doi.org/10.1186/bcr1650.
Liu, H., Sun, Q., Sun, Y., Zhang, J., Yuan, H., Pang, S., Qi, X., Wang, H., Zhang, M., Zhang, H., Yu, C., Gu, C., 2017. MELK and EZH2 cooperate to regulate medulloblastoma cancer stem-like cell proliferation and differentiation. Mol. Cancer Res. 15, 1275–1286. https://doi.org/10.1158/1541-7786.MCR-17-0105.
Liu, Z., Huang, L., Zhou, T., Chang, X., Yang, Y., Shi, Y., Hao, M., Li, Z., Wu, Y., Guan, Q., Zhang, W., Zuo, D., 2022. A novel tubulin inhibitor, 6h, suppresses tumor-associated angiogenesis and shows potent antitumor activity against non–small cell lung cancers. J. Biol. Chem. 298. https://doi.org/10.1016/j.jbc.2022.102063.
Ma, Y., Zhu, B., Liu, Xiaoguang, Yu, H., Yong, L., Liu, Xiao, Shao, J., Liu, Z., 2015. Inhibition of oleandrin on the proliferation and invasion of osteosarcoma cells *in vitro* by suppressing wnt/β-catenin signaling pathway. J. Exp. Clin. Cancer Res. 34, 115. https://doi.org/10.1186/s13046-015-0232-8.
Marie, S.K.N., Okamoto, O.K., Uno, M., Hasegawa, A.P.G., Oba-Shinjo, S.M., Cohen, T., Camargo, A.A., Kosoy, A., Carlotti, C.G., Toledo, S., Moreira-Filho, C.A., Zago, M.A., Simpson, A.J., Caballero, O.L., 2008. Maternal embryonic leucine zipper kinase transcript abundance correlates with malignancy grade in human astrocytomas. Int. J. Cancer 122, 807–815. https://doi.org/10.1002/ijc.23189.
Martucciello, S., Paolella, G., Romanelli, A.M., Sposito, S., Meola, L., Cerulli, A., Masullo, M., Piacente, S., Caputo, I., 2022. Pro-apoptotic and Pro-autophagic properties of cardenolides from aerial parts of pergularia tomentosa. Molecules. 27, 4874. https://doi.org/10.3390/molecules27154874.
Mbaveng, A.T., Bitchagno, G.T.M., Kuete, V., Tane, P., Efferth, T., 2019. Cytotoxicity of ungeremine towards multi-factorial drug resistant cancer cells and induction of apoptosis, ferroptosis, necroptosis and autophagy. Phytomedicine, 90th birthday of Professor Hildebert Wagner 60, 152832. https://doi.org/10.1016/j.phymed.2019.152832.
McDonald, I.M., Grant, G.D., East, M.P., Gilbert, T.S.K., Wilkerson, E.M., Goldfarb, D., Beri, J., Herring, L.E., Vaziri, C., Cook, J.G., Emanuele, M.J., Graves, L.M., 2020. Mass spectrometry–based selectivity profiling identifies a highly selective inhibitor

of the kinase MELK that delays mitotic entry in cancer cells. J. Biol. Chem. 295, 2359–2374. https://doi.org/10.1074/jbc.RA119.011083.
Mekhail, T., Kaur, H., Ganapathi, R., Budd, G.T., Elson, P., Bukowski, R.M., 2006. Phase 1 trial of Anvirzel in patients with refractory solid tumors. Invest. New Drugs 24, 423–427. https://doi.org/10.1007/s10637-006-7772-x.
Minata, M., Gu, C., Joshi, K., Nakano-Okuno, M., Hong, C., Nguyen, C.-H., Kornblum, H. I., Molla, A., Nakano, I., 2014. Multi-kinase inhibitor C1 triggers mitotic catastrophe of glioma stem cells mainly through MELK kinase inhibition. PLoS. One 9, e92546. https://doi.org/10.1371/journal.pone.0092546.
Murshed, M., Mares, M.M., Aljawdah, H.M.A., Al-Quraishy, S., 2024. *In vitro* evaluation of nerium oleander leaf extract against sarcoptes scabiei var. Cuniculi mite isolated from naturally infested rabbits. Indian J. Anim. Res. 58, 247–252. https://doi.org/10.18805/IJAR.BF-1725.
Nakano, I., Paucar, A.A., Bajpai, R., Dougherty, J.D., Zewail, A., Kelly, T.K., Kim, K.J., Ou, J., Groszer, M., Imura, T., Freije, W.A., Nelson, S.F., Sofroniew, M.V., Wu, H., Liu, X., Terskikh, A.V., Geschwind, D.H., Kornblum, H.I., 2005. Maternal embryonic leucine zipper kinase (MELK) regulates multipotent neural progenitor proliferation. J. Cell Biol. 170, 413–427. https://doi.org/10.1083/jcb.200412115.
Nasu, S., Milas, L., Kawabe, S., Raju, U., Newman, R., 2002. Enhancement of radiotherapy by oleandrin is a caspase-3 dependent process. Cancer Lett. 185, 145–151. https://doi.org/10.1016/s0304-3835(02)00263-x.
Newman, R.A., Kondo, Y., Yokoyama, T., Dixon, S., Cartwright, C., Chan, D., Johansen, M., Yang, P., 2007. Autophagic cell death of Human pancreatic tumor cells mediated by oleandrin, a lipid-soluble cardiac glycoside. Integr. Cancer Ther. 6, 354–364. https://doi.org/10.1177/1534735407309623.
Ni, Q., Miao, Y., Li, X., Yin, Z., Huang, H., Shi, G., Shi, W., 2024. Up-regulation of MELK promotes cell growth and invasion by accelerating G1/S transition and indicates poor prognosis in lung adenocarcinoma. Mol. Biotechnol. https://doi.org/10.1007/s12033-024-01143-4.
Olive, P.L., Banáth, J.P., 2006. The comet assay: a method to measure DNA damage in individual cells. Nat. Protoc. 1, 23–29. https://doi.org/10.1038/nprot.2006.5.
Omer, E.A., Abdelfatah, S., Riedl, M., Meesters, C., Hildebrandt, A., Efferth, T., 2023. Coronavirus inhibitors targeting nsp16. Molecules. 28, 988. https://doi.org/10.3390/molecules28030988.
Pickard, M.R., Green, A.R., Ellis, I.O., Caldas, C., Hedge, V.L., Mourtada-Maarabouni, M., Williams, G.T., 2009. Dysregulated expression of Fau and MELK is associated with poor prognosis in breast cancer. Breast Cancer Res. 11, R60. https://doi.org/10.1186/bcr2350.
Pitner, M.K., Taliaferro, J.M., Dalby, K.N., Bartholomeusz, C., 2017. MELK: a potential novel therapeutic target for TNBC and other aggressive malignancies. Expert. Opin. Ther. Targets. 21, 849–859. https://doi.org/10.1080/14728222.2017.1363183.
Plante, K.S., Dwivedi, V., Plante, J.A., Fernandez, D., Mirchandani, D., Bopp, N., Aguilar, P.V., Park, J.-G., Tamayo, P.P., Delgado, J., Shivanna, V., Torrelles, J.B., Martinez-Sobrido, L., Matos, R., Weaver, S.C., Sastry, K.J., Newman, R.A., 2021. Antiviral activity of oleandrin and a defined extract of *Nerium oleander* against SARS-CoV-2. Biomed. Pharmacother. 138, 111457. https://doi.org/10.1016/j.biopha.2021.111457.
Rascón-Valenzuela, L.A., Velázquez, C., Garibay-Escobar, A., Vilegas, W., Medina-Juárez, L.A., Gámez-Meza, N., Robles-Zepeda, R.E., 2016. Apoptotic activities of cardenolide glycosides from *Asclepias subulata*. J. Ethnopharmacol. 193, 303–311. https://doi.org/10.1016/j.jep.2016.08.022.
Rashan, L.J., Özenver, N., Boulos, J.C., Dawood, M., Roos, W.P., Franke, K., Papasotiriou, I., Wessjohann, L.A., Fiebig, H.-H., Efferth, T., 2023. Molecular modes of action of an aqueous nerium oleander extract in cancer cells *In vitro* and *In vivo*. Molecules. 28, 1871. https://doi.org/10.3390/molecules28041871.
Roth, T., Burger, A.M., Dengler, W., Willmann, H., Fiebig, H.H., 1999. Human tumor cell lines demonstrating the characteristics of patient tumors as useful models for anticancer drug screening. https://doi.org/10.1159/000425830.
Sanna, G., Madeddu, S., Serra, A., Collu, D., Efferth, T., Hakkim, F.L., Rashan, L., 2021. Anti-poliovirus activity of nerium oleander aqueous extract. Nat. Prod. Res. 35, 633–636. https://doi.org/10.1080/14786419.2019.1582046.
Secer Celik, F., Eroglu Gunes, C., Kurar, E., 2023. Cardiac glycoside oleandrin suppresses EMT ability in endometrial carcinoma cells. Int. J. Mol. Cell Med. 12, 220–228. https://doi.org/10.22088/IJMCM.BUMS.12.3.220.
Shi, J., Yang, C., An, J., Hao, D., Liu, C., Liu, J., Sun, J., Jiang, J., 2021. KLF5-induced BBOX1-AS1 contributes to cell malignant phenotypes in non-small cell lung cancer via sponging miR-27a-5p to up-regulate MELK and activate FAK signaling pathway. J. Exp. Clin. Cancer Res. 40, 148. https://doi.org/10.1186/s13046-021-01943-5.
Siegel, R.L., Miller, K.D., Wagle, N.S., Jemal, A., 2023. Cancer statistics, 2023. CA Cancer J. Clin. 73, 17–48. https://doi.org/10.3322/caac.21763.
Singhal, K.G., Gupta, G.D., 2011. Some Central nervous system activities of nerium oleander linn (Kaner) flower extract. Trop. J. Pharmaceut. Res. 10, 455–461. https://doi.org/10.4314/tjpr.v10i4.11.
Speers, C., Zhao, S.G., Kothari, V., Santola, A., Liu, M., Wilder-Romans, K., Evans, J., Batra, N., Bartelink, H., Hayes, D.F., Lawrence, T.S., Brown, P.H., Pierce, L.J., Feng, F.Y., 2016. Maternal embryonic leucine zipper kinase (MELK) as a novel mediator and biomarker of radioresistance in Human breast cancer. Clin. Cancer Res. 22, 5864–5875. https://doi.org/10.1158/1078-0432.CCR-15-2711.
Sudakin, V., Yen, T.J., 2007. Targeting mitosis for anti-cancer therapy. BioDrugs 21, 225–233. https://doi.org/10.2165/00063030-200721040-00003.
Tang, Q., Li, W., Zheng, X., Ren, L., Liu, J., Li, S., Wang, J., Du, G., 2020. MELK is an oncogenic kinase essential for metastasis, mitotic progression, and programmed death in lung carcinoma. Sig Transduct. Target Ther. 5, 1–12. https://doi.org/10.1038/s41392-020-00288-3.
Touré, B.B., Giraldes, J., Smith, T., Sprague, E.R., Wang, Y., Mathieu, S., Chen, Z., Mishina, Y., Feng, Y., Yan-Neale, Y., Shakya, S., Chen, D., Meyer, M., Puleo, D., Brazell, J.T., Straub, C., Sage, D., Wright, K., Yuan, Y., Chen, X., Duca, J., Kim, S., Tian, L., Martin, E., Hurov, K., Shao, W., 2016. Toward the validation of maternal embryonic leucine zipper kinase: discovery, optimization of highly potent and selective inhibitors, and preliminary biology insight. J. Med. Chem. 59, 4711–4723. https://doi.org/10.1021/acs.jmedchem.6b00052.
Verheye-Dua, F.A., Böhm, L., 2000. Influence of apoptosis on the enhancement of radiotoxocity by Ouabain. Strahlenther. Onkol. 176, 186–191. https://doi.org/10.1007/s000660050055.
Wang, D., Zou, F., Li, Y., Hu, J., Gao, L., 2024. Targeting MELK improves PD-1 blockade efficiency in cervical cancer via enhancing antitumor immunity. Mol. Ther. Oncol. 32. https://doi.org/10.1016/j.omton.2024.200759.
Wang, X., Spandidos, A., Wang, H., Seed, B., 2012. PrimerBank: a PCR primer database for quantitative gene expression analysis, 2012 update. Nucleic. Acids. Res. 40, D1144–D1149. https://doi.org/10.1093/nar/gkr1013.
Wang, Y., Li, Y.-M., Baitsch, L., Huang, A., Xiang, Y., Tong, H., Lako, A., Von, T., Choi, C., Lim, E., Min, J., Li, L., Stegmeier, F., Schlegel, R., Eck, M.J., Gray, N.S., Mitchison, T. J., Zhao, J.J., 2018. Correction: MELK is an oncogenic kinase essential for mitotic progression in basal-like breast cancer cells. Elife 7, e36414. https://doi.org/10.7554/eLife.36414.
Wen, S., Chen, Y., Lu, Y., Wang, Y., Ding, L., Jiang, M., 2016. Cardenolides from the *Apocynaceae* family and their anticancer activity. Fitoterapia 112, 74–84. https://doi.org/10.1016/j.fitote.2016.04.023.
Xia, H., Kong, S.N., Chen, J., Shi, M., Sekar, K., Seshachalam, V.P., Rajasekaran, M., Goh, B.K.P., Ooi, L.L., Hui, K.M., 2016. MELK is an oncogenic kinase essential for early hepatocellular carcinoma recurrence. Cancer Lett. 383, 85–93. https://doi.org/10.1016/j.canlet.2016.09.017.
Xu, Q., Ge, Q., Zhou, Y., Yang, B., Yang, Q., Jiang, S., Jiang, R., Ai, Z., Zhang, Z., Teng, Y., 2020. MELK promotes endometrial carcinoma progression via activating mTOR signaling pathway. EBioMedicine 51, 102609. https://doi.org/10.1016/j.ebiom.2019.102609.
Yu, H., Xu, X., Zhu, L., Chen, S., He, J., 2024. MELK aggravates lung adenocarcinoma by regulating EZH2 ubiquitination and H3K27me3 histone methylation of LATS2. J. Cell Mol. Med. 28, e18216. https://doi.org/10.1111/jcmm.18216.
Zang, X., Qian, C., Ruan, Y., Xie, J., Luo, T., Xu, B., Jiang, J., 2019. Higher maternal embryonic leucine zipper kinase mrna expression level is A poor prognostic factor in non-small-cell lung carcinoma patients. Biomark. Med. 13, 1349–1361. https://doi.org/10.2217/bmm-2019-0052.
Zhai, J., Dong, X., Yan, F., Guo, H., Yang, J., 2022. Oleandrin: a systematic review of its natural sources, structural properties, detection methods, pharmacokinetics and toxicology. Front. Pharmacol. 13, 822726. https://doi.org/10.3389/fphar.2022.822726.
Zhang, C., Li, Q., Qin, G., Zhang, Y., Li, C., Han, L., Wang, R., Wang, S., Chen, H., Liu, K., He, C., 2021. Anti-angiogenesis and anti-metastasis effects of Polyphyllin VII on hepatocellular carcinoma cells *in vitro* and *in vivo*. Chin. Med. 16, 41. https://doi.org/10.1186/s13020-021-00447-w.
Zhou, M., Boulos, J.C., Omer, E.A., Rudbari, H.A., Schirmeister, T., Micale, N., Efferth, T., 2023. Two palladium (II) complexes derived from halogen-substituted Schiff bases and 2-picolylamine induce parthanatos-type cell death in sensitive and multi-drug resistant CCRF-CEM leukemia cells. Eur. J. Pharmacol. 956, 175980. https://doi.org/10.1016/j.ejphar.2023.175980.